USP10 strikes down Wnt/β-catenin signaling by dual-wielding deubiquitinase activity and phase transition potential

Yinuo Wang[1,#], Aihua Mao[2,3,#], Jingwei Liu[4,#], Pengjie Li[5,#], Shaoqin Zheng[1], Tong Tong[1], Zexu Li[1], Haijiao Zhang[1], Lanjing Ma[1], Jiahui Lin[1], Zhongqiu Pang[1], Qing Han[1], Fukang Qi[5], Xinjun Zhang[6], Maorong Chen[7], Xi He[7], Xi Zhang[8], Teng Fei[1], Bi-Feng Liu[5], Daming Gao[9], Liu Cao[4,*], Qiang Wang[2,*], Yiwei Li[5,*], Ren Sheng[1,10,*]

[1]College of Life and Health Science, Northeastern University, Shenyang 110819, China.

[2]Division of Cell, Developmental and Integrative Biology, School of Medicine, South China University of Technology, Guangzhou 510006, China.

[3]Guangdong Provincial Key Laboratory of Marine Biotechnology, Institute of Marine Sciences, Shantou University, Shantou, Guangdong 515063, China.

[4]College of Basic Medical Science, China Medical University, Shenyang 110122, China.

[5]Key Laboratory for Biomedical Photonics of MOE at Wuhan National Laboratory for Optoelectronics - Hubei Bioinformatics and Molecular Imaging Key Laboratory, Department of Biomedical Engineering, College of Life Science and Technology, Huazhong University of Science and Technology, Wuhan 430074, China.

[6]Key Laboratory of Molecular Biophysics of the Ministry of Education, National Engineering Research Center for Nanomedicine, College of Life Science and Technology, Huazhong University of Science and Technology, Wuhan 430074, China.

[7]F.M Kirby Neurobiology Center, Boston Children's Hospital, Department of Neurology, Harvard Medical School, Boston, MA 02115, USA.

[8]College of Sciences, Northeastern University, Shenyang 110004, China.

[9]State Key Laboratory of Cell Biology, CAS Center for Excellence in Molecular Cell Science, Shanghai Institute of Biochemistry and Cell Biology, Chinese Academy of Sciences, Shanghai 200031, China.
[10]Lead contact
#These authors share equal contribution
*Correspondence: lcao@cmu.edu.cn (L.C.), qiangwang@scut.edu.cn (Q.W.), yiweili@hust.edu.cn (Y.L.), shengren@mail.neu.edu.cn (R.S.)

Abstract

Wnt/β-catenin signaling is a conserved pathway crucially governing development, tissue homeostasis and oncogenesis in metazoan. Through screening, we identified a deubiquitinase (DUB) USP10 as a novel modulator of Wnt/β-catenin signaling. Mechanistically, USP10 binds to Axin1 via conserved motifs and stabilizes Axin1 through K48-linked deubiquitination. And in parallel, USP10 tethers Axin1 and β-catenin physically, via stabilizing the phase separation of Axin1 through its intrinsically-disordered regions, which is regardless of its enzymatic activity. Functionally, we show USP10 prominently regulates zebrafish embryonic development and murine intestinal homeostasis by antagonizing Wnt/β-catenin signaling. Additionally in human colorectal cancer, USP10 substantially represses cancer growth and correlates with Wnt/β-catenin magnitude clinically. Collectively, we discovered USP10 functioning in multiple biological processes through repressing Wnt/β-catenin signaling and unearthed a novel DUB-dependent and -independent "dual-regulating" mechanism by which USP10 utilizes in Wnt regulation context-dependently. Our study also suggested the potential of USP10 inhibitor in treating Wnt-related diseases.

Key words: USP10, Wnt/β-catenin signaling, phase separation, development, organoid, colorectal cancer.

Introduction

Wnt/β-catenin signaling (aka canonical Wnt signaling) is a pivotally conserved signaling cascade in metazoans[1,2]. In vertebrate, Wnt/β-catenin signaling critically governs multiple biological processes including embryonic development and adult tissue homeostasis. Mechanistically, in the absence of Wnt ligand, co-transcription factor β-catenin is contained within the "destruction complex" primarily composed by Axin1 and APC (*Adenomatous Polyposis Coli*), therefore undergoes phosphorylation by GSK3 (Glycogen Synthase Kinase 3)/CK1 (Casein Kinase 1) and ends up with ubiquitination and proteasomal degradation. While Wnt ligand is present, it binds and recruits (co-)receptors to form signalosome on the plasma membrane and disrupts the presence of Axin1 and GSK3 in the destruction complex. As a result, β-catenin becomes released from its confinement, then translocating into the nucleus to initiate the expression of target genes that regulate cell proliferation, differentiation, and self-renewal. Dysregulation of Wnt/β-catenin signaling causes severe developmental disorders, degenerative diseases and malignant tumors, in particular colorectal cancers (CRC)[1,2]. Though the core of this signaling cascade has been studied for decades, discovery of new regulators is still of great value for both basic and translational medicine. For instance, as novel findings, Rspo and Notum greatly expanded the mechanistic understanding of Wnt signaling regulation, as the antibody or inhibitor against them has been proven promising for particular cancer treatments[3-9].

As a central component of Wnt/β-catenin signaling, Axin1 is indispensable for both Wnt activation and β-catenin suppression[1]. It contains RGS domain for APC engagement, a conserved helix for β-catenin binding and DIX domain for multimerization with Dishevelled, while the majority remains unstructured (presumably intrinsically-disordered). However, thanks to this flexibility, Axin1 has been shown capable of either undergoing phase separation or polymerization, which effectively facilitates the entrapment of β-catenin within the destruction complex[10].

Regulation of Axin1 critically depends on the post-translational modifications (PTM).

For instance, the phosphorylation at S497 allows Axin1 to obtain an "open" conformation to make full contact with β-catenin[11]. Tankyrase (TNKS) can regulate the protein stability by poly-ribosylating Axin1 amino-terminal, which allows Axin1 subsequent ubiquitination by RNF146 for degradation[12-14]. TNKS inhibitor such as XAV939, shows promise in treating Wnt-dependent diseases by regulating Axin1 protein level[12]. Other regulators of Axin1 post-translational modification were also reported, which play important roles in Wnt signaling tranduction[15-19].

Ubiquitination is a protein PTM that rules cellular protein degradation and activities[20]. By dynamic elongation or removal of K48-linked ubiquitin chain, the fate of protein can be decided for degradation or preservation, which is crucially required for cellular protein homeostasis. Additionally, other residues-linked (K63, K27, and etc.) ubiquitination were known to affect the protein activity. As one of the well-studied deubiquitinases (DUBs), USP10 has been shown to regulate multiple important biological processes[21]. It was reported that USP10 deubiquitinates substrates including FLT3, PTEN, KLF4 and YAP/TAZ to regulate cancer growth[22-25]. Other literatures also show that USP10 can deubiquitinate p53, VPS34 complex, NOTCH and AMPK in various biological conditions[26-29]. The small molecule inhibitor of USP10, Spautin-1, has been shown for translational medical potentials in treating various diseases[27,30].

In this study, we have identified USP10 as a critical suppressor of Wnt/β-catenin signaling through cDNA screening. Notably, USP10 dominates Wnt/β-catenin signaling via dual paths. USP10 can directly associate with both β-catenin and Axin1 via conserved motifs and remarkably stabilize Axin1 through K48-specific deubiquitination. And unexpectedly, USP10 can also corroborate the puncta formation of Axin1 through physical constraining-mediated phase separation, which is independent of its DUB activity. These two paths work parallelly and context-dependently. In terms of biological functions, we find that USP10 plays crucial roles in embryonic development and intestinal homeostasis by modulating the amplitude of Wnt/β-catenin signaling via DUB activity. And in human CRC, USP10 significantly

116 represses tumor progression mainly through enzymatic-independent function both *in*
117 *vitro* and *in vivo*, and correlates with patient survival and Wnt magnitude clinically.
118 Taken together, we have identified that USP10 directly regulates Wnt/β-catenin
119 signaling for the first time and revealed a novel DUB-dependent and -independent
120 "dual-wielding" mechanism. By employing multiple biological models, we have fully
121 elucidated the functional significance of USP10 on Wnt regulation, and suggest the
122 therapeutic promise for treating developmental and regenerative defects by using
123 USP10 inhibitor.
124
125 **Results**
126 **USP10 is a negative regulator of Wnt/β-catenin signaling**
127 We performed DUBs cDNA screening under Wnt3a conditioned medium (CM)
128 stimulation by exercising TOPFlash reporter (B/R system) as readout to identify novel
129 DUBs that potentially regulate Wnt/β-catenin signaling. To obtain reliable results, we
130 used two different transfection levels of cDNA as two independent experiment sets
131 and included stringent controls in the screen. Amongst the initially screened 30 DUBs,
132 we found that USP10 had a strong inhibitory effect on Wnt/β-catenin signaling which
133 was comparable to that of Axin1 (**Fig.1a, S1a**). This inhibitory effect of ectopically
134 expressed USP10 on Wnt/β-catenin signaling was then validated in human CRC cells
135 (**Fig.S1b, S1c**). To further consolidate the results, we showed that USP10 inhibited
136 Wnt/β-catenin signaling in a dose-dependent manner presented by both the luciferase
137 assay and cytosolic β-catenin level (**Fig.1b, 1c**). Knockout or knockdown of USP10,
138 on the contrary, activated Wnt/β-catenin signaling as shown in various assays,
139 including TOPFlash reporter and the accumulation of cytoplasm β-catenin (**Fig.1d,**
140 **1e, S1d-S1h**). To exclude the possibility that USP10 affects Wnt/β-catenin through
141 other related pathways, we employed dual-luciferase chemiluminescence to detect the
142 changes of target genes including TGFβ, BMP, CREB and etc. The result showed that
143 expression of USP10 had little effect on these pathways, thus strongly suggested that
144 USP10 exerts suppression on Wnt/β-catenin directly (**Fig.S1i**).

145 Next, we sought to elucidate the mechanism. To effectively unravel the complexity of
146 Wnt/β-catenin signaling, we first used GSK3 inhibitor CHIR99021 to divide Wnt/β-
147 catenin cascade into the upstream (Wnt signalosome formation) and the downstream
148 events (β-catenin destruction complex formation and afterwards) (**Fig.1f**). After
149 treatment of CHIR99021, USP10 still showed significant inhibition on Wnt/β-catenin
150 signaling that was comparable to Axin1, indicating that the manner of USP10
151 functioning was independent of Wnt signalosome formation (**Fig.1g**). Meanwhile, we
152 constructed the N-terminal truncated β-catenin (ΔN-β-catenin), a mutant commonly
153 used as the constitutively active variant due to absence of GSK3 and CK1
154 phosphorylation sites. By comparing the wild-type (WT) β-catenin and ΔN-β-catenin,
155 we showed that USP10 was only able to effectively inhibit Wnt/β-catenin signaling
156 during WT β-catenin overexpression but not ΔN-β-catenin, which indicated that
157 USP10 could not significantly affect β-catenin nuclear transportation (**Fig.1h, S1j**).
158 Taken together, we have identified USP10 as a novel negative regulator of Wnt/β-
159 catenin signaling and argued that USP10 functions at the β-catenin destruction
160 complex level.
161
162 **USP10 stabilizes Axin1 through K48-linked deubiquitination**
163 Next, we examined the interaction of USP10 with the key components of the
164 destruction complex (including β-catenin, Axin1, APC, GSK3 and β-Trcp). By
165 employing co-immunoprecipitation (co-IP), we observed that USP10 interacted with
166 β-catenin, Axin1 and GSK3 at both exogenous and endogenous levels (**Fig.2a, S2a**).
167 Since USP10 was a repressor of Wnt/β-catenin signaling, we intuitively focused on
168 Axin1 and logically hypothesized that USP10 might regulate Axin1 ubiquitination and
169 stability. We first showed that endogenous Axin1 protein level could be upregulated
170 upon treatment of the proteasome inhibitor MG132 (**Fig.2b**). At the presence of
171 ectopic USP10, the stability of Axin1 was significantly enhanced regardless of
172 MG132 while Axin1 transcription level remained unaltered (**Fig.2b, S2b**).
173 Interestingly, the presence of USP10 showed even stronger improvement of Axin1

protein level than protease inhibitor, which suggested USP10 might have other functions beyond Axin1 deubiquitination. This Axin1-increasing effect was also dose-dependent on USP10 level (**Fig.S2c**). To check the protein stability of Axin1, pulse-chase assay was exercised by blocking the *de novo* protein synthesis and observing the turnover of the existing protein. We found that USP10 overexpression significantly enhanced endogenous Axin1 stability, as USP10 depletion showed the opposite effect (**Fig.2c, S2d, S2e**). The inhibitory effect of USP10 on Wnt/β-catenin was significantly attenuated when Axin1 was knocked-down, indicating that USP10 regulates Wnt/β-catenin signaling mainly through Axin1 (**Fig.2d, S2f**).

In terms of Axin1 ubiquitination, USP10 depletion resulted in aggravated Axin1 ubiquitination, which could be recovered by USP10 rescue (**Fig.2e, S2g**). It was further confirmed that Axin1 was a direct substrate of USP10 via *in vitro* deubiquitination assay (**Fig.S2h**). Moreover, USP10 mainly removed K48-linked ubiquitination on Axin1, which was consistent with its regulation on Axin1 stability (**Fig.2f**). The effect was lost when we employed USP10-CA (USP10 C424A, enzymatically-dead mutant)[27], suggesting USP10 deubiquitinates Axin1 based on its DUB activity (**Fig.S2h, 2g, S2i**). Based on the binding results, we also showed USP10 could not deubiquitinate β-catenin (**Fig.S2j**). This result brought clear evidence that USP10 serves unambiguously as Wnt/β-catenin signaling antagonist, unlike another DUB, USP7, which stabilizes both Axin1 and β-catenin as previously reported[15,31]. On the other hand, we employed the USP10 inhibitor Spautin-1 to validate our results through chemical perturbation. The addition of Spautin-1 enhanced the ubiquitination of Axin1, destabilized Axin1 and inhibited the activity of the Wnt/β-catenin, which drew consistent conclusions with the genetic manipulations (**Fig.2h, S2k, S2l**).

We then mapped the binding site between USP10 and Axin1. Topologically, USP10 contains two major parts: a conserved DUB domain at its carboxyl terminal as the rest of the protein forms one lengthy non-structured region at its amino terminal (named as ΔDUB) (**Fig.2i**). We therefore constructed and expressed USP10 full-length (FL),

203 CA, DUB and ΔDUB *in vitro* and performed pull-down experiments. It was clearly
204 seen that USP10 FL, CA and ΔDUB interacted with Axin1 as USP10 DUB domain
205 alone lost the binding capacity (**Fig.2j, S3a**). Since the ΔDUB was unstructured, we
206 arbitrarily divided it into four pieces with approximate 100 amino acids for each,
207 named Segment 1-4 (S1-S4), respectively (**Fig.2i**). By employing the pull-down and
208 co-IP assays, we found that S2 was mainly responsible for Axin1 binding (**Fig.2k,**
209 **S3b**). Since Wnt/β-catenin signaling is highly conserved, we argued that the binding
210 between USP10 and Axin1 should involve in their conserved residues. Through the
211 alignment of USP10 in different species, we found seven conserved motifs within the
212 ΔDUB (**Fig.S3c**). Through co-IP and pull-down assays, we confirmed the USP10
213 binding site was a conserved polybasic region (PBR) in S2 region (a.a. 143-163)
214 (**Fig.2l, S3d**).
215 We further divided Axin1 into six parts based on earlier study (**Fig.S3e**) [11]. From co-
216 IP and pull-down assays, we found that USP10 mainly interacted with the putative
217 CK1 binding region and DIX domain (**Fig.2m, S3f**). It was previously report that
218 Axin1 DIX domain contains a negatively-charged patch that forms self-inhibition
219 intramolecularly [11]. Thus, we hypothesized that this patch was responsible for USP10
220 PBR binding through electrostatic interaction. We observed that the binding between
221 Axin1 and USP10 was significantly alleviated when we mutated the negatively-
222 charged patch to neutral residues (Axin1-DA) or we truncated the USP10 PBR
223 (ΔPBR) (**Fig.2n**). It was further confirmed that losing either the PBR on USP10 or the
224 negatively-charged patch on Axin1 caused loss-of-function effect of USP10 in Axin1
225 ubiquitination and stabilization (**Fig.2o, S3g**). Taken together, USP10 directly binds to
226 Axin1 through its conserved PBR. Axin1 is a direct substrate of USP10 for K48-
227 linked deubiquitination which leads to the ensuing Axin1 stabilization.
228
229 **USP10 acts as a scaffold in β-catenin destruction complex**
230 While elucidating the deubiquitination of Axin1 by USP10, we noticed another
231 interesting phenomenon. Despite the lack of DUB activity, expression of USP10-CA

232 and USP10-ΔDUB consistently reduced TOPFlash reporter activity in a moderate
233 manner instead of behaving dominant-negative (**Fig.3a**). From knockout and rescue
234 experiment, the same phenomenon was seen (**Fig.3b, 3c**). We thus hypothesized USP10
235 might affected Wnt/β-catenin signaling besides Axin1 deubiquitination. First, we
236 verified that neither USP10-CA nor -ΔDUB could deubiquitinate Axin1 (**Fig.S4a**).
237 However, USP10-CA and -ΔDUB could reduce cytoplasmic β-catenin in a dose-
238 dependent manner (**Fig.3d, S4b**). Together with the finding that USP10 interacted with
239 multiple components of the β-catenin destruction complex, we proposed that USP10-
240 ΔDUB may function as a scaffold that physically enhances the complex formation like
241 Amer1/WTX[32-34]. When we looked into the USP10-β-catenin interaction, we found
242 USP10 S1 and S4 were responsible, which primarily bound to 1-5 and 9-12 Armadillo
243 repeats on β-catenin (**Fig.3e, S4c-S4f**). Gradient transfection of ΔDUB led to increased
244 interaction between Axin1 and β-catenin dose-dependently (**Fig.3f, 3g**). USP10
245 depletion, on the other hand, reduced the binding between Axin1 and β-catenin
246 endogenously (**Fig.S4g**). In brief, we proposed that USP10 bound to Axin1 mainly by
247 the conserved residues in S2 and to β-catenin by S1 and S4. S2 is absolutely required
248 for both DUB-dependent and -independent activity of USP10 as it is the only region
249 capable of Axin1 binding. S1 and S4 are responsible for β-catenin engagement for
250 DUB-independent activity of USP10, which are not required for Axin1 deubiquitination.
251 In line with our hypothesis, the minimal inhibitory units and dominant negative mutants
252 were validated by the luciferase assays (**Fig.3h, S4h**).
253

254 **USP10 facilitates the puncta formation of Axin1 via a IDRs-mediated phase**
255 **separation-like manner independent of DUB activity**

256 After we dissected the contribution of USP10 in the physical interaction between Axin1
257 and β-catenin, we investigated the stabilization of Axin1 granule. The formation of
258 Axin1 granule was supposed to form via either IDR (intrinsically disordered region) -
259 mediated liquid-liquid phase separation of DIX domain-mediated oligomerization in
260 previous literatures[10]. As we tested above, the interaction between the Axin1 and USP10

261 happened between the DIX domain and PBR of USP10 via multivalent electrostatic
262 interactions. Briefly, the PBR of USP10 was a lengthy non-structured IDR, while
263 electrically neutralized DIX domain efficiently prevented the interaction without
264 affecting the original function of the DIX domain[11]; these results suggested that the
265 stabilization of USP10 on Axin1 granule taken place mechanistically through an IDRs-
266 mediated phase separation-like process rather than DIX domain mediated heat-to-tail
267 polymerization. Meanwhile, we want to note that the physically phase separation and
268 polymerization favors each other[35-37], which might augment the stabilization of Axin1
269 granule in the downstream. Nevertheless, our live imaging of Axin1-mCherry clearly
270 showed their dynamic fusion and splitting of the formed droplet-like structure (**Fig.S5a**).
271 A fluorescence recovery after photobleaching (FRAP) assay further confirmed the
272 condensates of Axin1 maintained its recovery capability (**Fig.S5b, S5c**)[38]. From the
273 assay of FRAP, we showed that the Axin1 granule contained both the recoverable
274 fraction and immobile fraction, which suggested it contained both the DIX domain-
275 mediated polymerization and phase separation from physical interaction.
276 To study whether USP10 could regulate the granule formation of Axin1, we
277 simultaneously expressed USP10 and Axin1 (**Fig.4a**). Co-expression with USP10 led
278 to more Axin1 granules per cell together with larger sizes as compared to Axin1
279 transfection alone (**Fig.4b, 4c**). In addition, we analyzed the immobile faction of Axin1
280 in the condensates using FRAP assay to reflect the irreversibility in the Axin1-mCherry
281 granules. A larger immobile fraction indicated that stabler Axin1 granules were
282 obtained with overexpressed USP10 (**Fig.4d**). An opposite trend was obtained when we
283 depleted the endogenous USP10 by shRNA (**Fig.4b-4d**). To further confirm that it was
284 the non-structured region-mediated phase separation assisting the granule formation of
285 Axin1, we showed that USP10-ΔDUB still promoted the granule formation of Axin1,
286 which confirmed that the importance of the physical interaction in its function. As noted,
287 unlike the USP10 FL, USP10-ΔDUB was not able to deubiquitinate and elevate the
288 cellular contents of the Axin1, thus, USP10-ΔDUB elevated the granule formation of
289 Axin1 fully on its non-structured region-mediated phase separation instead of

290 increasing the concentration of Axin1 at the first place. More significantly, USP10-
291 ΔDUB exhibited an even stronger promotion effect on the granule formation of Axin1
292 as compared to the full-length USP10 (**Fig.4b-4d**), which might suggest the non-
293 structured region-mediated phase separation has a more direct effect as compared to the
294 deubiquitinating functionality. This result clearly indicated that the ΔDUB was
295 sufficient for the granule augmentation via phase separation. Consistently, USP10-CA
296 stabilized the granules of Axin1 as shown by their larger size (**Fig.4c**) and their
297 increased immobile fraction under FRAP (**Fig.4d**), despite of the similar numbers of
298 Axin1 granule per cells formed as compared to USP10 WT (**Fig.4b**). One could argue
299 that USP10-CA was more efficient to coalesce small Axin1 puncta into larger ones and
300 the number of puncta did not increase.
301 We also exercised additional assays to substantiate the findings. First, we employed
302 immunofluorescence to observe the endogenous puncta formation of Axin1. The
303 experiment was performed in SW480 cells, in which endogenous Axin1 formed puncta
304 as described by the previous literature[39]. We knocked out the endogenous USP10 by
305 CRISPR-Cas9 and rescued with Myc-tagged WT or mutant USP10 to the
306 approximately equal level of the endogenous protein (**Fig.S5d, S5e**). The results
307 illustrated that in the absence of USP10, Axin1 puncta number was significantly
308 reduced (**Fig.4e, 4f**). Rescue by either USP10 WT, CA or ΔDUB could recover the
309 puncta formation of endogenous Axin1 (**Fig.4e, 4f**). Also, we performed *in vitro*
310 droplet/condensate formation assay to further dissect the role of USP10 in regulating
311 Axin1 phase separation. We expressed mCherry-tagged Axin1 and GFP-tagged USP10
312 (WT and mutants) in *E. coli* and purified the proteins by chromatography. It was clearly
313 seen that Axin1 droplet size significantly enlarged after co-incubation with USP10 WT,
314 CA or ΔDUB (**Fig.4g, 4h**). The fluorescent microscopy also showed strong co-
315 existence of the red and green channels. As the negative control, ΔDUB ΔPBR (internal
316 truncation of PBR in ΔDUB region) neither could coexist with Axin1 nor promote
317 Axin1 droplet formation (**Fig.4e-4h**). Together, we conclude that the USP10 stabilizes
318 the puncta of Axin1 via phase separation independent of its DUB activity but relying

319 on the intrinsically-disordered region.

320 Next, we tested whether the enhancement effect of USP10 on Axin1 granule via phase
321 separation was through the multivalent physical interactions. As we mentioned above,
322 Axin1-DA, which contains a negative-charged patch in DIX domain turning into
323 neutral residues, exhibited a significantly suppressed binding to USP10 (**Fig.2o**). As
324 compared to Axin1 WT, we further showed that the number, the diameter and the
325 stability of Axin1-DA puncta were significantly lessened (**Fig.S5f-S5g,4i**). More
326 importantly, overexpression of either USP10 WT or USP10-ΔPBR no longer promotes
327 the formation of Axin1-DA puncta, as no phase separation between Axin1 and USP10
328 can be elevated after eliminating the multivalent physical interactions in Axin1-DA
329 (**Fig.4i**). Thus, our results suggested that USP10-Axin1 physical interactions are mainly
330 responsible for the enhancement of granule via phase separation. Based on these finding,
331 we argue that USP10 directly augments the Axin1-containing puncta through its IDRs-
332 mediated phase separation, which could enhance the formation of β-catenin destruction
333 complex in the downstream regardless of the DUB activity[10]. We proposed a
334 mechanistic model that USP10 may repress Wnt/β-catenin signaling via two parallel
335 paths. USP10 can stabilize Axin1 through its DUB activity and meanwhile physically
336 connect the key components in the β-catenin destruction complex through a phase
337 separation-like effect (**Fig.4j**). Each path individually or synergistically contributes to
338 the repressive effect of USP10 on Wnt/β-catenin signaling.

339

340 **USP10 functions in embryonic dorsoventral patterning and axis formation**
341 **through Wnt/β-catenin signaling**

342 The potential roles of USP10 in embryonic development are poorly understood.
343 Zebrafish has emerged as a powerful model to investigate embryonic development
344 due to its external fertilization and transparent embryos. To gain insight into the
345 functions of USP10 during zebrafish embryonic development, we firstly examined its
346 expression by whole-mount *in situ* hybridization with an antisense probe. As shown in
347 (**Fig.S6a**), zebrafish *usp10* transcript was ubiquitously detected in embryos from the

348 one-cell stage up to the early somite stage. Interestingly, the expression of *usp10* was
349 predominantly found in the developing eye field at 24 hours post-fertilization (hpf),
350 which was remarkable decreased at 36 hpf. These results indicate that *usp10* is a
351 maternal and zygotic gene and might have potential roles in early embryonic
352 development. We then assessed the effects of human USP10 (hUSP10)
353 overexpression on embryogenesis. Over 80% of the embryos injected with wild-type
354 hUSP10 mRNA displayed ventralized phenotypes at 24 hpf, including a variably
355 reduced head and notochord and expanded ventral tissues (**Fig.5a, 5b**).
356 To further confirm the role of USP10 in the embryonic dorsal-ventral pattering, the
357 expression of dorsal markers, such as *bozozok (boz)* and *goosecoid* (*gsc*) were
358 analyzed at the sphere stage by *in situ* hybridization. We found that overexpression of
359 hUSP10 led to decreased expression of *boz* and *gsc* (**Fig.5c, 5d**). Meanwhile, the
360 expansion of ventral non-neural ectoderm (indicated by *gata2* expression) further
361 revealed the dorsal-ventral defects in hUSP10 overexpressed embryos (**Fig.5e**). On
362 the contrary, expression of the DUB-dead mutant, USP10-CA, showed minor effect as
363 compared to WT USP10 (**Fig.5b-5e**). Inhibition of the DUB activity of endogenous
364 USP10 in wild-type embryos by treatments with Spautin-1 obviously strengthened the
365 expression of dorsal marker genes and repressed the expression of ventral gene *gata2*
366 in a dose-dependent manner (**Fig.5f-5h**). These results suggest that USP10 functions
367 in embryonic dorsal-ventral patterning mainly via its DUB activity.
368 Previous studies have demonstrated that maternal Wnt/β-catenin signaling is essential
369 for dorsal-ventral patterning during embryogenesis[40-42]. Given that our findings from
370 cell culture systems indicated that USP10 inhibits Wnt signaling, we asked whether
371 USP10 would affect embryonic dorsoventral axis formation through regulating
372 Wnt/β-catenin pathway. To do this, hUSP10 mRNA was injected into transgenic
373 embryos expressing GFP reporter under TCF/LEF/β-catenin responsive promoter
374 (TOPdGFP)[43]. Results from *in situ* hybridization experiments revealed that hUSP10
375 overexpression remarkably reduced the GFP reporter expression in the dorsal
376 organizer, suggesting a defective activation of Wnt/β-catenin signaling (**Fig.5i**). On

377 the other hand, blocking the DUB activities of endogenous USP10 in *Tg(TOPdGFP)*
378 embryos by Spautin-1 treatment strongly enhanced GFP expression (**Fig.5j**).
379 Furthermore, the reduced expression of dorsal marker genes *gsc* and *boz* in hUSP10
380 overexpressed embryos were well restored by co-injection with *ΔN-β-catenin* mRNA
381 (**Fig.5k, 5l**). These data suggested that USP10 has a profound impact on maternal
382 Wnt/β-catenin signaling during early embryonic development. In addition, consistent
383 with the data *in vitro*, immunoblotting results showed an obvious increase of
384 endogenous zebrafish Axin1 protein level in embryos with hUSP10 overexpression
385 (**Fig.S6b, S6c**). In contrast, inhibition of the deubiquitinate activity of USP10 resulted
386 in a significant decrease of Axin1 (**Fig.S6d, S6e**). Altogether, these results indicate
387 that USP10 has a conserved role in regulating Axin1 stability depending on its DUB
388 activity, which is responsible for proper dorsoventral axis patterning during embryo
389 development.
390
391 **USP10 critically regulates intestinal organoid homeostasis**
392 Intestinal organoid (mini-gut) culturing emerges as an essential tool to study intestinal
393 homeostasis *ex vivo*[44-46]. It is a three-dimensional structure that consists intestinal-
394 specific cell types and cell lineage and can recapitulate the growth and differentiation
395 of intestinal epithelium. The sphere-like organoid represents the clustering of $Lgr5^+$
396 intestinal stem cells and the budded organoid represents the well-differentiated
397 epithelial mini-structure. It is well established that intestinal organoid growth and
398 differentiation are highly dependent on Wnt/β-catenin signaling amplitude[44,46]. In
399 intestinal "stem cell" state culture (sphere-like), we initially found that the organoid
400 could not survive from the overexpression of USP10, which prevented us from
401 statistical analysis. We therefore employed the "Tet-off" system to study the effect.
402 When doxycycline was removed from the medium, we found that ectopic expression
403 of USP10 led to the straight intestinal stem cell death similar to the effect of Axin1,
404 and this phenotype could be rescued by the addition of GSK3 inhibitor (**Fig.6a, 6b**).
405 Under such circumstance, overexpression of USP10-CA only showed partial effect in

resulting cell death (**Fig.6a, 6b**). When USP10 was depleted in differentiated intestinal organoid culture (budded), the organoid architecture changed as the number of sphere-like bodies was markedly increased (**Fig.6c, 6d, S7a, S7b**). This change of stemness was further evidenced by the increase of proliferation marker Ki67 and reduction of differentiation marker Krt20 (**Fig.6c**). And this effect could be effectively reversed by the addition of TNKS inhibitor XAV939 (**Fig.6c, 6d)**. While we used Spautin-1 to inhibit USP10 DUB activity in intestinal organoid culture, we noticed a significant increase in the number of sphere-like bodies which represented the increase of self-renewal potential (**Fig.6e, 6f, S7c, S7d**). However, the diameters of Spautin-1 treated spheres were significantly smaller than those of GSK3 inhibitor, which indicated their difference in potentiating stem cell growth and suggested the scaffolding and phase-transitional function of USP10 could have potential influence in this situation (**Fig.6g, S7e-S7i**). Together, these results indicate that USP10 modulates intestinal organoid growth and differentiation *ex vivo* through Wnt/β-catenin signaling. Both the DUB activity and biophysical property of USP10 contribute to the intestinal organoid homeostasis. USP10 inhibitor such as Spautin-1 possesses therapeutic potential in regeneration for Wnt/β-catenin stimulation.

USP10 suppresses CRC growth through inhibition of Wnt/β-catenin signaling

Wnt/β-catenin dysregulation is the predominant cause for human CRC[47]. APC mutation takes up to 80-85% in all CRC as RNF43 (an E3 ubiquitin ligase that degrades Wnt receptors) mutation and Rspo (a morphogen antagonizing RNF43) superfusion fill up the rest space[48-50]. We thus assessed the role of USP10 in CRC. We first verified that in CRC cell lines, ectopic expression of USP10 effectively increased endogenous Axin1 level and reduced cytosolic β-catenin amount, as depletion of USP10 behaved oppositely (**Fig.7a-7c, S8a**). Functionally, we found that ectopic expression of USP10 significantly inhibited CRC cell growth both two- and three-dimensionally, as well as cancer cell migration, whereas USP10 depletion (both knockout and knockdown) or overexpression of the dominant-negative USP10 mutants accelerated cancer growth

435 instead (**Fig.7d-7g, S8b-S8f**). Notably, expression of the DUB-dead mutant, USP10-
436 CA, was capable to effectively mitigate the cancer growth comparable to the effect of
437 USP10 WT (**Fig.7d, 7f, 7g**). Molecularly, USP10-CA reduced the cytosolic β-catenin
438 level and Wnt-target genes (Wnt feedback: AXIN2 and LGR5; cell proliferation: MYC
439 and CCND1) to the same extent of USP10 WT (**Fig. 7h, 7i**). This data demonstrates the
440 enhancement effect of USP10 on physical phase separation but not USP10 DUB
441 activity is mainly required to withhold CRC growth. And we thus logically argue that
442 the USP10-mediated anti-tumor effect in CRC mainly depends on its inhibition on
443 Wnt/β-catenin instead of other pathways, given the fact that all other tumor-suppressing
444 USP10 functions known previously rely on its DUB activity[21,51].
445 We next transplanted these cells subcutaneously onto nude mice for *in vivo* study. For
446 the transplanted DLD-1 cells, the size and weight of the derived tumors were
447 significantly increased when USP10 was depleted (**Fig.7j, 7k, S8g**). In contrast, either
448 USP10 WT or USP10-CA overexpression caused significant diminish of the *in vivo*
449 tumor growth, which was consistent with the *in vitro* results (**Fig.7j, 7k, S8g**). The
450 immunohistochemistry (IHC) showed stronger staining for Ki67 and β-catenin in
451 shUSP10 group than the control group (**Fig.7l**). And the intensities of these staining
452 were attenuated when either USP10 WT or USP10-CA was ectopically expressed (**Fig.**
453 **7l**).
454 To further consolidate the role of USP10 in CRC, we looked into the clinical database
455 and acquired the human tumor specimens. From TCGA database, we found that
456 USP10 expression showed significant positive correlation with longer overall survival
457 in CRC patients (**Fig.S8h**). This correlation in prognosis was also supported by
458 another research which studied a Korean CRC cohort[52]. To determine the
459 consequence of differential expression of USP10 in human CRC, 92 primary CRC
460 tissues on a microarray were examined by IHC. Representative images were shown in
461 **Fig.7m**. The grouped analysis based on USP10 intensity showed clear difference in
462 Axin1 and nuclear β-catenin ratio in the CRC samples (**Fig.S8i, S8j**). Overall, higher
463 USP10 level significantly correlated with higher Axin1 level and lower nuclear-

localized β-catenin ratio, which was fully supportive to our molecular and cell biological studies (**Fig.7m-7o**). Collectively, our data has shown that USP10 suppresses CRC growth by inhibiting Wnt/β-catenin both *in vitro* and *in vivo*, and the DUB-independent scaffolding function plays the major role in CRC growth blockade. Clinically, USP10 level significantly correlates with CRC patient survival, Axin1 levels and nuclear β-catenin ratio.

Discussion

Wnt/β-catenin signaling is an essential pathway that is being actively studied for decades[1,2]. For the first time, we identified USP10 as a critical regulator of this pathway and proved that USP10 participates in various Wnt-governed biological processes. In embryonic development and intestinal homeostasis, perturbation of USP10 showed strong Wnt-related phenotypes. And in CRC, USP10 behaves as a strong tumor suppressor both *in vitro* and *in vivo* and shows correlation in the clinical investigations.

As a "star molecule" that was reported to regulate multiple important proteins[21], the biological significance and multipurpose nature of USP10 are further revealed in this work. However, different from the previous researches, we have discovered a novel mechanism that USP10 regulates Wnt/β-catenin signaling by both classical (DUB activity) and alternative (scaffolding and phase transition) paths. USP10 directly binds to Axin1 through each other's conserved motifs, which enables the clearance of K48-linked ubiquitination on Axin1 to lengthen the protein lifetime. This binding, on the other hand, occupies the Axin1 intramolecular inhibition site on the DIX domain and potentially allows the "open-state" of Axin1 to further extend for β-catenin entrapment[11]. Also, the intrinsically-disordered region of USP10 bridges both Axin1 and β-catenin, therefore offers USP10 a scaffold position in the dynamic formation of the destruction complex. As a result, USP10 is crucially for the physical interaction in phase separation process and the recruitments of β-catenin. This novel "dual-

492 wielding" mechanism sheds new light on the versatility of USP10 functions and
493 provides new directions for researchers who are interested in DUB studies.
494 The dual Wnt-regulatory mechanisms of USP10 both rely on Axin1, but can act
495 parallelly to modulate the magnitude of Wnt signaling. We also observed that in
496 different biological processes, the functional significance of each "weapon" was
497 highly context-dependent. For instance, in embryonic development, dorsal-ventral
498 axis formation and patterning primarily require the DUB activity. Both the enzymatic
499 and scaffolding capabilities are involved in intestinal homeostasis, whereas in human
500 CRC the scaffolding capability of USP10 is more predominant. One reason could be
501 that in diverse contexts, the sensitivity of Axin1 stabilization and destruction complex
502 formation are different. This might result in the redundancy of one path and the dearth
503 of the other. Therefore, the dominance of particular activity or the coordination of
504 both in various biological situations requires further scrutiny. Once these processes
505 are fully understood, one could envision that USP10 inhibitor such as Spautin-1, may
506 have therapeutic potentials in particular tissue maintenance, organ regeneration or
507 degenerative disease treatment. And small molecules blocking USP10 PBR binding
508 with Axin1 might have even broader potential applications in Wnt-defective disease
509 therapy.
510 Many aspects can affect the malignant tumor progression. In our study, USP10
511 downregulates Wnt/β-catenin signaling to reduce cell stemness and decelerate cell
512 cycle [1]. Alternatively, USP10 was also reported to inhibits cancer growth by
513 deubiquitinating tumor suppressors including PTEN, AMPK and TP53[23,24,26-28,51]. So
514 presumably USP10 may affect CRC growth through these proteins. However, the
515 DUB-dead mutant, USP10-CA, which could not deubiquitinate any substrate rather
516 than elevate β-catenin degradation via physical phase separation, showed
517 indistinguishable effect to WT USP10 in Wnt/β-catenin suppression and CRC growth
518 inhibition. We thus argue that USP10 represses CRC growth mainly through Wnt/β-
519 catenin. To conclude, we have proved that USP10 substantially thwarts Wnt/β-catenin
520 signaling in various biological conditions through a novel dual-regulation mechanism.

Our work holds great value in basic biomedical research as well as potential for translation.

There are still certain issues for us to dissect in the near future. First, the functions of USP10 in different organ development and homeostasis are not fully studied in this work. Thus, USP10 (conditional) knockout and transgenic animals should be generated to obtain more tissue-specific and physiological results. Second, the relationship between USP10 DUB-dependent and -independent mechanisms in different biological processes needs further scrutiny. It is necessary to better understand the factors in each biological context and then correlate USP10 functionality of individual path.

Acknowledgement

The authors thank Dr. Chen Ding (Northeastern University) for scientific advice; Dr. Aina He (Shanghai Sixth People's Hospital) and Dr. Long Zhang (Zhejiang University) for plasmids sharing. R.S. acknowledges the support by the Fundamental Research Fund for the Central Universities, China N182005006 (completed), the Starting Funds for "100-talent plan" of Northeastern University, National Natural Science Foundation of China 31970721 and 81902830, and Liaoning Provincial Talents Project XLYC1807239 (completed). Y.L. acknowledges the National Natural Science Foundation of China 32171248 and 12102142, and the Fundamental Research Funds for the Central Universities, HUST grant 2021GCRC056. Q.W. acknowledges the support of National Natural Science Foundation of China 32025014 and 81921006. L.C. acknowledges the support by the key project of the National Natural Science Foundation of China 82030091.

Author contributions

R.S. designed the study. Y.W., A.M., J.L., P.L., S.Z., T.T., Z.L., H.Z., L.M., J.L., Q.H., F.Q. Y.L. and R.S. performed experiments and collected and analyzed the data. X.Z (Xinjun Zhang)., M.C., X.H., X.Z (Xi Zhang)., T.F., B.L., L.C., Q.W., Y.L., D.G. and

R.S. wrote and revised the manuscript. L.C., Q.W., Y.L. and R.S. oversaw the study. All authors have approved the manuscript.

Declarations of interest

The authors declare no conflict of interest.

Figure legends

Figure 1. USP10 is a negative regulator of Wnt/β-catenin signaling.

(a) DUB cDNA screening on Wnt/β-catenin signaling by TOPFlash reporter fold changes in HEK293T cell. The two axes represent two independent sets of experiments. LRP6 and β-catenin are positive controls, while ZNRF3 and Axin1 are negative controls.

(b) USP10 significantly reduces TOPFlash activity fold change dose-dependently at the presence of Wnt3a CM. Error bars mean ± SD, n = 3, two-tailed Student's t-test.

(c) USP10 reduces cytosolic β-catenin accumulation dose-dependently shown by WB assay.

(d) Knockout of USP10 significantly enhances TOPFlash reporter at the presence of Wnt3a CM. Error bars mean ± SD, n = 3, two-tailed Student's t-test.

(e) WB assay showing the alteration of cytosolic β-catenin levels under USP10 overexpression or knockout condition.

(f) Schematic flow of Wnt/β-catenin signal transduction process.

(g) TOPFlash reporter assay under the treatment of GSK3 inhibitor CHIR99021. ZNRF3: Wnt signalosome control. Axin1: β-catenin destruction complex control. Error bars mean ± SD, n = 3, two-tailed Student's t-test.

(h) TOPFlash reporter assay under the expression of wild-type and ΔN-β-catenin. Error bars mean ± SD, n = 3, two-tailed Student's t-test.

RLU: Relative Luciferase Unit. ns, not significant.

Figure 2. USP10 stabilizes Axin1 through K48-linked deubiquitination.

579 (a) Co-IP assay showing USP10 interaction with Axin1, β-catenin and GSK3
580 endogenously.
581 (b) Axin1 protein level changes under the expression of USP10 or/and the treatment
582 of proteasome inhibitor MG132.
583 (c) Pulse-chase assay of endogenous Axin1 under USP10 overexpression (upper) or
584 depletion (lower) conditions.
585 (d) Axin1 and cytosolic β-catenin levels under Axin1 knockdown or/and USP10
586 overexpression condition.
587 (e) Ubiquitination assay of Axin1 under USP10 knockdown and rescue conditions.
588 (f) Ubiquitination assay showing USP10 mainly affects Axin1 K48-ubiquitination.
589 (g) Ubiquitination assay showing USP10-CA mutant loses the capability to
590 deubiquitinate endogenous Axin1.
591 (h) Ubiquitination assay showing USP10 inhibitor Spautin-1 effectively thwarts
592 USP10 DUB activity and increases Axin1 ubiquitination level.
593 (i) Schematic diagram of USP10 truncation mutants constructed in this work.
594 (j, k) *In vitro* pull-down assay of different GST-USP10 fragments with Axin1.
595 Asterisks represent the major bands of the desired proteins.
596 (l) Co-IP assay of Axin1 with different conserved regions of USP10.
597 (m) Co-IP assay of USP10 with different segments of Axin1.
598 (n) Co-IP assay of USP10 WT/ΔPBR with Axin1 WT/DA.
599 (o) Ubiquitination assay showing USP10-ΔPBR cannot deubiquitinate Axin1. And
600 Axin1-DA cannot be deubiquitinated by USP10.
601
602 **Figure 3. USP10 acts as a scaffold in β-catenin destruction complex**
603 (a, b) TOPFlash reporter assay showing USP10-CA and USP10-ΔDUB retain
604 moderate inhibitory effect on Wnt/β-catenin by overexpression (a) or USP10
605 knockout and rescue (b). Error bars mean ± SD, n = 3, two-tailed Student's t-test.

(c) USP10 protein level test by WB in (b). The endogenous USP10 antibody cannot identify ΔDUB region and thus immunoblotting on Myc serves as a ruler for protein level.

(d) WB showing cytosolic β-catenin level diminishes dose-dependently of USP10-CA.

(e) Co-IP assay showing different segments of USP10 interacting with β-catenin.

(f, g) Co-IP assay showing the interaction strength of endogenous Axin1 and β-catenin enhances while the dose of USP10-ΔDUB increases.

(h) TOPFlash reporter assay showing the minimal functional truncations of USP10 require S2 region with the DUB domain. Error bars mean ± SD, n = 3, two-tailed Student's t-test.

Figure 4. USP10 facilitates the puncta formation of Axin1 via a IDRs-mediated phase separation-like manner independent of DUB activity

(a) Representative fluorescent images of Axin1 droplets when co-expressed with shCtrl, shUSP10, EV, USP10 WT, USP10 CA and USP10-ΔDUB.

(b-d) Numbers of Axin1 puncta per cell (b), size of Axin1 puncta (c), and immobile fraction (d) of Axin1 puncta. Error bars mean ± SD, two-tailed Student's t-test.

(e) Representative figures of Axin1 puncta by immunostaining of endogenous Axin1 in SW480 cell. Red, Axin1(Alexa 555). Blue, DAPI. All figures are in the same scale in this panel.

(f) The statistical analysis of (e). Error bars mean ± SD, by two-tailed Student's t-test.

(g) Representative figures of *in vitro* phase separation assay by co-incubation of bacterial expressed Axin1-mCherry and USP10-GFP (WT and mutants). Red, Axin1-mCherry. Green, USP10-GFP. All figures are in the same scale in this panel.

(h) The statistical analysis of (g). Error bars mean ± SD, by two-tailed Student's t-test.

(i) Immobile fraction of Axin1-DA puncta when co-expressed with USP10 WT and USP10-ΔPBR, as compared to Axin1 WT puncta.

(j) Working model of USP10 inhibiting Wnt/β-catenin signaling. The DUB activity contributes to deubiquitination and stabilization of Axin1, and the unstructured region promotes LLPS of the destruction complex through physical interactions.
RLU: Relative Luciferase Unit. ns, not significant.

Figure 5. USP10 functions in embryonic dorsoventral patterning and axis formation through Wnt/β-catenin signaling

(a, b) Embryos were injected with 500pg hUSP10 or hUSP10-CA mRNA at the one-cell stage. Representative embryos of different classes at 24 hpf were shown in (a), lateral views with anterior to the left. The percentage of embryos with indicated phenotype were shown in (b). Scale bar, 200μm.
(c-e) The expression analysis of dorsal marker genes (c, *boz* and d, *gsc*) at the sphere stage and ventral marker gene (e, *gata2*) in embryos injected with indicated mRNA at the 75% epi (epiboly) stage. Lateral views. Embryos were injected with 500pg hUSP10 or hUSP10-CA mRNA at one-cell stage, 500pg GFP injection was used as a control.
(f-h) Dorsal marker genes (f, *boz* and g, *gsc*) and ventral marker gene (h, *gata2*) were assessed in DMSO and Spautin-1 (5μmoL or 10μmoL) incubated embryos at indicated stage by *in situ* hybridization. Lateral views.
(i, j) Whole-mount *in situ* hybridization analyzed the transcript of gfp in hUSP10-injected (i) or Spautin-1 (j) treated *Tg(TOPdGFP)* embryos at shield stage. Animal views with dorsal side to the right. Red arrows point to the dorsal organizer of the embryo.
(k, l) Overexpression of *ΔN-β-catenin* mRNA rescued hUSP10-induced ventralization. Embryos were injected with 500pg of hUSP10 mRNA alone or together with 100pg of *ΔN-β-catenin* mRNA at the one-cell stage and harvested at the sphere stage for *in situ* hybridization with the probe of *gsc* (k) and *boz* (l).
The number of the embryos was indicated within each panel.

Figure 6. USP10 critically regulates intestinal organoid homeostasis

(a) Representative images (brightfield and red fluorescence) of murine intestinal organoids under different conditions. Dox: doxycycline.

(b) Quantitative analysis of the surviving/dead organoids percentage in a. Control group:n=65, USP10 WT group:n=71, USP10 CA group:n=67, Axin1 group:n=67, USP10 WT+CHIR99021 group:n=60.

(c) Representative images (brightfield and immunofluorescence) of murine intestinal organoids under USP10 depletion and XAV939 addition. Blue, DAPI; red, Ki67; green, Krt20.

(d) Quantitative analysis of the surviving/dead organoids percentage in c. shControl group:n=66, shUSP10 group:n=67, shUSP10+XAV939 group:n=68.

(e, f) Representative images (brightfield and immunofluorescence) of murine intestinal organoids under DMSO, Spautin-1 or CHIR99021 treatment. Blue, DAPI; red, Ki67; green, Krt20.

(g) Organoid (sphere-like) diameters quantifications in e shown by histogram. Error bars mean ± SD, n = 22, by two-tailed Student's t-test.

All images in any individual panel are in the same amplification scale except the individually marked ones.

Figure 7. USP10 suppresses CRC growth through inhibition of Wnt/β-catenin signaling.

(a-c) Endogenous Axin1 and cytosolic β-catenin levels in CRC cell lines under USP10 overexpression or depletion condition. (a) DLD-1, (b) HT29, (c) SW480.

(d, e) MTT cell growth assay of DLD-1, HT29 and SW480 cells under USP10 WT and USP10-CA overexpression (d) or USP10 depletion condition (e). Error bars mean ± SD, n = 3, two-way ANOVA.

(f, g) Colony formation assays of DLD-1 (f) and HT29 (g) under USP10 WT/CA overexpression or USP10 depletion condition.

691 (h) Endogenous Axin1 and cytosolic β-catenin levels in DLD-1 cells with
692 overexpression of WT USP10 and USP10-CA.
693 (i) RT-qPCR assay of Wnt target genes expression, including LGR5, AXIN2, MYC
694 and CCND1 in DLD-1. Error bars mean ± SD, n = 3, two-tailed Student's t-test.
695 (j, k) Quantitative analyses of the tumor volume (j) and weight (k) of subcutaneously
696 transplanted DLD-1 cells. Tumor volume: Error bars mean ± SD, n = 10 for each
697 group, by two-way ANOVA analysis. Tumor weight: Error bars mean ± SD, n = 10 for
698 each group, by two-tailed Student's t-test analysis.
699 (l) Representative IHC staining images of β-catenin and Ki67 of the tumor formed
700 from subcutaneously transplanted DLD-1 cell.
701 (m) Representative IHC staining images of Axin1 and β-catenin in CRC patients in
702 USP10-high (upper row) and USP10-low (lower row) groups.
703 (n, o) The correlations of USP10 with Axin1 (n) and nuclear localized β-catenin ratio
704 (o) in CRC patients. By two-tailed Spearman correlation analysis. All images in any
705 individual panel are in the same amplification scale. ns, not significant.
706

707 **Materials and Methods**

708 **Key resources table**

REAGENT or RESOURCE	**Source**	**Identifier**
Antibodies		
USP10(D7A5) Rabbit mAb	Cell Signaling Technology	#8501
Axin1(C76H11) Rabbit mAb	Cell Signaling Technology	#2087
V5-Tag (D3H8Q) Rabbit mAb	Cell Signaling Technology	#13202
HA-Tag (C29F4) Rabbit mAb	Cell Signaling Technology	#3724
Myc-Tag (9B11) Mouse mAb	Cell Signaling Technology	#2276
DYKDDDDK Tag (D6W5B) Rabbit mAb	Cell Signaling Technology	#14793
Anti-GFP Rabbit mAb	Proteintech	50430-2-AP
β-Catenin (D10A8) XP® Rabbit mAb	Cell Signaling Technology	#8480
β-Catenin (L87A12) Mouse mAb	Cell Signaling Technology	#2698

GSK-3β (27C10) Rabbit mAb	Cell Signaling Technology	#56500
GSK-3β (3D10) Mouse mAb	Cell Signaling Technology	#9832
Anti-Gapdh Rabbit	Proteintech	10494-1-AP
Ki-67 (8D5) Mouse mAb	Cell Signaling Technology	#9499
KRT20 Rabbit pAb	ABclonal	A17997
Anti-mouse IgG, HRP-linked Antibody	Cell Signaling Technology	#7076
Anti-rabbit IgG, HRP-linked Antibody	Cell Signaling Technology	#7074
β-catenin (E5) Mouse mAb	Santa Cruz Biotechnology	sc-7963
Goat anti-Rabbit IgG (H+L) Highly Cross-Adsorbed Secondary Antibody, Alexa Fluor 488	Invitrogen	A-11034
Goat anti-Mouse IgG (H+L) Highly Cross-Adsorbed Secondary Antibody, Alexa Fluor 555	Invitrogen	A-21422
Goat anti-Rabbit IgG (H+L) Highly Cross-Adsorbed Secondary Antibody, Alexa Fluor 555	Invitrogen	A-21429
Bacterial strand		
E. coli NEB® 5-alpha	New England Biolabs (NEB)	C2987H
E. coli-BL21	New England Biolabs (NEB)	C2530H
Commercial chemicals and biologics		
Cycloheximide	Sigma-Aldrich	5087390001
CHIR99021	Cayman	13122
Thiazolyl Blue Tetrazolium Bromide	Sigma-Aldrich	M5655
Hoechst	Thermo	1990363
Puromycin	Invivogen	ant-pr-1
Geneticin	Invivogen	ant-gn-1
Gibco™ Penicillin-Streptomycin-Glutamine (100X)	Gibco	10378016
Polybrene	Santa Cruz Biotechnology	SC-134220
MG132	Beyotime Biotechnology	S1748

Spautin-1	Beyotime	SC5498
Poly-L-lysine	Sango Biotech	A600751
Crystal violet	Sango Biotech	A100528
Neofect™ DNA transfection reagent	Neofect	ME201901
Ampicillin	Sango Biotech	A100339
4% paraformaldehyde	Beyotime Biotechnology	P0099
Tris[(1-benzyl-1H-1,2,3-triazol-4-yl) methyl] amine	Sigma-Aldrich	678937
Digitonin	Sigma-Aldrich	D141
Triton X-100	Sigma-Aldrich	X100
IGEPAL® CA-630	Sigma-Aldrich	I3021
β-D-thiogalactoside (IPTG)	Beyotime Biotechnology	ST098
TrypLE™ Express Enzyme (1X), no phenol red	Gibco	12604021
B-27™ Supplement (50X), minus vitamin A	Gibco	12587010
N-2 Supplement (100X)	Gibco	17502048
EGF Recombinant Mouse Protein	Gibco	PMG8041
N-Acetyl-L-cysteine	Sigma-Aldrich	A9165
Nicotinamide	Sigma-Aldrich	N0636
Y-27632	Sigma-Aldrich	Y0503
Recombinant Murine Noggin	Peprotech	250-38
Corning® Matrigel® Growth Factor Reduced (GFR) Basement Membrane Matrix, Phenol Red-free, *LDEV-free	Corning	356231
PEG8000	Sango Biotech	A600433
Kanamycin sulfate	Sango Biotech	A600286
HEPES	Beyotime	ST092
Imidazole	Sigma-Aldrich	I5513
Reduced glutathione	Sigma-Aldrich	V900456
Critical commercial assays/kits		
Dual Luciferase Reporter Gene Assay Kit	Beyotime Biotechnology	RG027
Endo-free Plasmid Mini Kit	Omega	D6950
UNlQ-10 Column Trizol Total RNA Isolation Kit	Sango Biotech	B511321

MonScript™ RTIII All-in-One Mix with dsDNase	Monad	MR05101M
MonAmp™ ChemoHS qPCR Mix	Monad	MQ00401S
GeneJET Gel Extraction Kit	Thermo	K0692
GeneJET PCR Purification Kit	Thermo	K0702
Phanta Max Super-Fidelity DNA Polymerase	Vazyme	P505-d1
Chemistar™ High-sig ECL Western Blotting Substrate	Tanon	180-5001
GST Fusion Protein Purification Kit	Genscript	L00206
mMessage mMachine kit	Ambion	AM1348
MEGAscript Kit	Ambion	AM1626
Experimental models: Cell lines		
HEK293T	ATCC	CRL-11268 RRID:CVCL_1926
HEK293T BAR/Renilla (B/R)	This study	
L cell	ATCC	CRL-2648
L-Wnt3a cell	ATCC	CRL-2647
RKO	ATCC	CRL-2577
RKO BAR/Renilla (B/R)	This study	
DLD-1	NCACC, China	TCHu134
DLD-1 BAR/Renilla (B/R)	This study	
HT29	Procell	CL-0118
SW480	NCACC, China	TCHu172
Experimental models: Animals		
BALB/cA-nude mice	Beijing HFK Bioscience CO.,LTD	13001A
C57BL/6J mice	Beijing HFK Bioscience CO.,LTD	11001A
Zebrafish wild-type Tubingen strain	[43]	
Zebrafish *Tg(TOPdGFP)* strain	[43]	
Oligonucleotides		
Control-shRNA sequence	This study	AAAAAAAAAAAAAAAAAAAAA

#1-shUSP10 sequence(human)	[26]	GCCTCTCTTTAGTGGCTCTTT
#2-shUSP10 sequence(human)	[26]	CCTATGTGGAAACTAAGTATT
#1-shUSP10 sequence(mouse)	[53]	CGCAGAGGAGTATCTAGGTTT
#2-shUSP10 sequence(mouse)	This study	GCAGAGTTATTGGAGACTGTA
#1-shAxin1 sequence(human)	This study	CCCGTGTAAATATGTACATTT
#2-shAxin1 sequence(human)	This study	GAGGAGAAGATCATCGGCAAA
CTNNB1-RT-qPCR primers	This study	F:AAAGCGGCTGTTAGTCACTGG R:CGAGTCATTGCATACTGTCCAT
AXIN2-RT-qPCR primers	This study	F:AGCCAAAGCGATCTACAAAAGG R:AAGTCAAAAACATCTGGTAGGCA
ZNRF3-RT-qPCR primers	This study	F:GGGTCATCCCCTGTACTCAC R:TTGTCCTCGTAGGGTAGGCTG
LGR5-RT-qPCR primers	This study	F:CTCCCAGGTCTGGTGTGTTG R:GAGGTCTAGGTAGGAGGTGAAG
MYC-RT-qPCR primers	This study	F:GTCAAGAGGCGAACACACAAC R:TTGGACGGACAGGATGTATGC
CCND1-RT-qPCR primers	This study	F:CAATGACCCCGCACGATTTC R:CATGGAGGGCGGATTGGAA

GAPDH-RT-qPCR primers	This study	F:GGAGCGAGATCCCTCCAAAAT R:GGCTGTTGTCATACTTCTCATGG
USP10-RT-qPCR primers	This study	F:GAGGGCACAGCTACCAACG R:AGGGGAGATATGGCGGGAG
AXIN1-RT-qPCR primers	This study	F:GGTTTCCCCTTGGACCTCG R:CCGTCGAAGTCTCACCTTTAATG
USP10 sgRNA sequence	PMID: 31748695	GCCTGGGTACTGGCAGTCGA
USP10 sgRNA primer for sanger sequence	This study	F:ACACTTTGCCGAGAACC R:TAGCTGTAATATCCAGG
Recombinant DNA		
Lenti-EF1α-puro Myc-USP10	This study	
Lenti-EF1α-puro Flag-Axin1	This study	
Lenti-EF1α-puro V5-Axin1	This study	
Lenti-EF1α-puro Flag-β-catenin	This study	
Lenti-EF1α-puro mCherry-Axin1	This study	
Lenti-EF1α-puro Flag-LRP6	This study	
Lenti-EF1α-puro HA-ZNRF3	This study	
Lenti-EF1α-puro GFP-APC	This study	
Lenti-EF1α-puro GFP-GSK3	This study	
Lenti-EF1α-puro Flag-β-Trcp	This study	
PGEX4T-1-USP10	This study	
PGEX4T-1-Axin1	This study	
pGIPZ-puro-tet-off-USP10	This study	
pGIPZ-puro-tet-off-Axin1	This study	
pLKO-puro shUSP10	This study	
pLKO-puro shAxin1	This study	

Lenti-EF1α-puro V5-Ub	This study	
pCMV-VSV-G	Addgene	#8454
psPAX2	Addgene	#12260
pCS2 ΔN-β-catenin	This study	
pCS2 human DUB cDNA library	This study	
pcDNA3.1 SRE reporter	Addgene	#82686
pGL3 BRE luciferase	Addgene	#45126
pGL3 CAGA reporter	Gifted by Dr. Long Zhang	[54]
7TFP	Addgene	#24308
pGL3-Renilla luciferase	This study	
pGL2 (basic) 3xARE Lux	Addgene	#14934
pSV232AL-5xGal4-CREB-TATA	Addgene	#46756
Lenti-Cas9-puro	Addgene	#108100
Lenti-Cas9-puro sgUSP10	This study	
pET28a	Novagen	69864
pET28a-Axin1	This study	
pET28a-β-catenin	This study	
pGEX4T-1-Axin1-mCherry	This study	
pGEX4T-1-USP10-GFP	This study	
pGEX4T-1-USP10-CA-GFP	This study	
pGEX4T-1-USP10-ΔDUB-GFP	This study	
pGEX4T-1-USP10-ΔDUB-ΔPBR-GFP	This study	
Software and algorithms		
Graphpad Prism 8	Graphpad software	https://www.graphpad.com
ImageJ	[55]	https://imagej.nih.gov/ij/
PhotoShop CC2019	Adobe	https://www.adobe.com/cn/products/photoshop.html
Other		
Protein G Plus- Agarose	Santa Cruz Biotechnology	SC-2002
α-Myc Agarose Affinity Gel	Sigma-Aldrich	7470
α-Flag Agarose Affinity Gel	Sigma-Aldrich	4596
EQKLISEEDL (Myc-tag) peptide	Sangon Biotech	Custom synthesis
Ni-NTA resin	Genscript	L00250
GST resin	Genscript	L00206

EXPERIMENTAL MODEL AND SUBJECT DETAILS

Human specimen study

The tissue microarrays of 92 cases of colon adenocarcinoma (OD-CT-DgCol04) were purchased from Shanghai Outdo Biotech Company, China. The research approach of immunohistochemical detection of protein expression in tissues of colon cancer has been approved by the Ethics Committee of China Medical University (Permission no: [2021] 206).

Animal Work

Mice: All mice were purchased from Beijing HFK Bioscience CO., LTD. Mice maintenance and treatments described were approved by the Research Ethics Committees of the College of Life and Health Sciences of Northeastern University (Approval no. NEU-EC-2021A018S and NEU-EC-2022A019S).

Zebrafish strains: The adult fishes were raised under standard conditions. Embryos were obtained from natural mating, which were grown at 28.5°C in Holtfreter's solution, and staged according to the morphology as previously described [56]. Adult wild-type (Tubingen strain) and *Tg(TOPdGFP)* [43] were used in this study. The experiments performed were approved by the Animal Care and Use Committee at the Institute of Zoology, Chinese Academy of Sciences (Permission Number: IOZ-13048).

Subcutaneous tumor transplantation

DLD-1 cells were trypsinized and resuspended in DMEM. Nude mice (Beijing HFK Bioscience CO., LTD) were subcutaneously injected at a density of 1×10^6 DLD-1 cells per site, and the designed cell number and viability were determined using trypan blue.

Murine intestinal crypt isolation

Mice after anesthesia treatment were sacrificed by cervical dislocation, and 2-3cm portions of the proximal intestine were collected, opened longitudinally and washed with ice-cold PBS. The luminal side was scraped to remove luminal contents and

villous structures. After washing again with ice-cold PBS, the intestine was cut into 2-5mm pieces with scissors. The intestinal fragments were then incubated in 2mM EDTA/PBS on ice for 30min. EDTA was then removed, which was followed by 10mL of cold PBS addition for sequel manual suspension for 3min to release the crypt. The supernatant was collected and passed through a 70μm filter (FALCON) to remove tissue debris. After three washes with PBS and centrifugation at 600g to remove tissue debris, the crypts were enriched in the resulting pellet and subsequently embedded in Matrigel gels (Corning).

Cell lines

This study utilized HEK293T, DLD-1, RKO, HT29, SW480, L and L-Wnt3a cells. All cell lines were maintained in humidified incubators with 5% CO_2 at 37°C. HEK293T (parental and genetically modified), DLD-1 (parental and genetically modified), RKO (parental and genetically modified), SW480 (parental and genetically modified), L and L-Wnt3a cells were cultured in DMEM-High Glucose supplemented with 10% FBS (fetal bovine serum) and 100mg/mL of penicillin/streptomycin/glutamine (Gibco). HT29 cells (parental and genetically modified) were cultured in RPMI-1640 medium supplemented with 10% FBS and 100mg/mL of penicillin/streptomycin/glutamine (Gibco).

METHOD DETAILS

Clones and constructs

Expressing Myc-tagged USP10 plasmids (wild-type and mutants), Flag-tagged Axin1 plasmid (wild-type and mutants), Flag -tagged β-catenin plasmid (wild-type and mutants), mCherry-tagged Axin1 plasmids were constructed in customized Lenti-EF1α-puro vector. Plasmids containing shControl, shUSP10 and shAxin1 were constructed in pLKO vector (primer sequence in reagent). Expressing GST-tagged USP10 plasmids (wild-type and mutants) and GST-tagged Axin1 plasmids (wild-type and mutants), GST-tagged USP10-GFP plasmids (wild-type and mutants) and GST-tagged Axin1-mCherry were constructed in pGEX-4T-1 vector. USP10 WT, USP10-CA, Axin1 were constructed in customized pGIPZ-tet-off-puro vector. His6-tagged

767 Axin1 and His6-tagged β-catenin were constructed in pET28a vector. The plasmid
768 containing sgUSP10 was constructed in Lenti-Cas9-puro vector (sequence in the
769 reagent). All plasmids were transformed in *E. coli* NEB®5α chain for amplification
770 and extracted by OMEGA Endo-free Plasmid Mini Kit. The concentrations of all
771 plasmids were determined by Thermo Nanodrop 2000.

772 **Cell culture and transfection**

773 HEK293T, RKO, L and L-Wnt3a cells were purchased from ATCC. DLD-1 and
774 SW480 cells were purchased from the NCACC, China. HT29 were purchased from
775 Procell.

776 HEK293T (parental and genetically modified), RKO (parental and genetically
777 modified), DLD-1 (parental and genetically modified), SW480 (parental and
778 genetically modified), L and L-Wnt3a cells were cultured in DMEM Medium
779 supplemented with 10% FBS and 100mg/mL of penicillin/streptomycin/glutamine.
780 HT29 cells (parental and genetically modified) were cultured in RPMI1640 medium
781 with 10% FBS and 100mg/mL penicillin/streptomycin/glutamine.

782 Transfection was done using Neofect. Transient cDNA transfection was performed
783 using Neofect according to the manufacturer's recommendations. Plasmids were
784 diluted using DMEM and mixed with Neofect. The complexes were incubated for 20
785 min at room temperature (RT) and added to HEK293T (parental or modified) cells in
786 growth medium. After 24-48hrs, cells were lysed using Passive Lysis Buffer (25mM
787 Tris-HCl, 150mM NaCl, 0.5% CA630).

788 **Lentivirus production and infection**

789 For lentivirus production, psPAX2 (for packaging, Addgene) and pCMV-VSV-G (for
790 enveloping, Addgene) and the desired plasmid constructed in the custom Lenti-EF1α-
791 puro vector or Lenti-Cas9-puro sgUSP10 were co-transfected in HEK293T cells at a
792 mass ratio (ng) of 5:1:5. After transfection for 24hrs, the medium was carefully
793 aspirated and replaced with fresh medium to produce virus-containing conditioned
794 medium. Virus can be harvested at 48, 72, and 96hrs post transfection. For lentiviral
795 infection, cell cultures were added to 0.5-1mL of conditioned medium containing

796 virus, 1mL fresh medium and polybrene (Santa Cruz Biotech, 1:1000). After 48hrs,
797 the medium was gently aspirated from the cells and replaced with fresh medium
798 containing appropriate antibiotics for resistance selection.

799 **Cell line generation**

800 HEK293T BAR/Renilla (B/R) cell line, RKO BAR/Renilla (B/R) cell line and DLD-1
801 BAR/Renilla (B/R) cell line: HEK293T cells, RKO cells or DLD-1 cells were
802 infected with lentiviruses containing 7TFP and Renilla for 48hrs. After that, the
803 medium was removed and replenished with fresh medium containing puromycin
804 (Invivogen) and geneticin (Invivogen) for selection for 72hrs. Eventually, selected
805 cells were cultured in normal medium and verified by dual luciferase reporter assay.
806 USP10 KO cell lines: The selected sgRNA sequence
807 (GCCTGGGTACTGGCAGTCGA) were cloned into Lenti-Cas9-puro vectors
808 (Addgene). HEK293T or SW480 cells stably expressing Lenti-Cas9-puro sgUSP10
809 were generated following lentiviral infection and puromycin resistance selection.
810 After reaching confluency, cells were digested and diluted to approximately one
811 cell/well, and seeded into 96-well plates to generate single clone in HEK293T or
812 SW480 cells. Genotypes of single cell clones were determined by both sequencing
813 DNA fragments containing targeted sgRNA regions amplified using sgUSP10 sanger
814 sequence PCR primers and immunoblotting against USP10 antibody (see Reagents or
815 Resource).

816 **Antibodies and immunoblotting**

817 Antibodies were purchased from different companies (see detail in Reagents and
818 Resources: Antibodies). Cells were lysed by passive lysis buffer (25mM Tris-HCl,
819 150mM NaCl, 0.5% CA630) containing protease inhibitor cocktail (Roche). The cells
820 were lysed in SDS loading buffer and boiled for 5-10min, followed by 8% or 10%
821 poly-acrylamide gel for SDS-PAGE. For Western blotting, all primary antibodies were
822 used at a 1:1000 dilution and all secondary antibodies were used at a 1:5000 dilution.
823 Chemiluminescent substrate kit was purchased from GE and Tanon. Final
824 quantification of gel intensity was done by ImageJ and plotted in Prism 8.0.

825 **Immunoprecipitation**

826 For co-immunoprecipitation, total lysates of cells were incubated with α-Flag-agarose
827 or α-Myc-agarose overnight at 4°C. Next day, the resins were washed thoroughly five
828 times with lysis buffer incubated and shaken for 10min at 4°C and resuspended in
829 SDS loading buffer, boiled for 5min, used for the SDS-PAGE and Western blotting.

830 **Reverse transcription and quantitative real-time PCR**

831 UNlQ-10 Column Trizol Total RNA Isolation Kit (Sango Biotech) was used to extract
832 total RNA from cells and reverse transcribed by MonScript™ RTIII All-in-One Mix
833 with dsDNase (Monad) according to the manufacturer's protocol. Quantitative RT-
834 PCR (qPCR, for RNA) and PCR (for genomic DNA) were performed using
835 MonAmp™ ChemoHS qPCR Mix (Monad). All primers are designed based on the
836 primer bank of Massachusetts General Hospital (https://pga.mgh.harvard.edu/cgi-
837 bin/primerbank). All experiments were performed in triplicate. The expression values
838 were normalized to those of GAPDH. PCR primer sequences are listed in the
839 "Reagents or Resource".

840 **Pulse-chase assay**

841 The cells in 24-well plates (with 70-80% confluency) were treated with
842 cycloheximide (Sigma-Aldrich) 300μg/mL at a range of time points (i.e., 0, 2, 4, 6,
843 8hrs). Cells were harvested at indicated time points and lysates were prepared and
844 analyzed. Afterwards, the gel intensity was quantified by ImageJ and fitted into first
845 order decay, and protein half-life ($t_{1/2}$) was calculated according to $\ln(N)-\ln(N_0) = -kt$
846 linear equation. k=degradation rate constant (min^{-1}).

847 **L conditioned medium (LCM) and L-Wnt3a conditioned medium (Wnt3aCM)**

848 L cells and L-Wnt3a cells were grown in DMEM medium supplemented with 10%
849 FBS. L cells expressing Wnt3a were cultured to 80-90% confluency and collected
850 every 2 days for 6 days. Maximal activity was determined using the TOPFlash assay
851 for subsequent Wnt stimulation experiments. Conditioned medium from L cells
852 collected as control.

853 **TOPFlash Dual-luciferase reporter assay**

For TOPFlash reporter assays, the TOPFlash reporter cell line (HEK293T B/R, cells containing stably expressed superTOPFlash (BAR) and *Renilla* (internal control) vectors) were used. Cells were seeded in 48-well plates and used Neofect for transfect, each set was repeated three times. For experiments requiring Wnt3a stimulation, the medium was changed to 1:1 mixed fresh medium and Wnt3aCM or LCM. After 18 hours of stimulation, dual-luciferase reporter assays were performed using the Dual Luciferase Reporter Assay Kit (Beyotime Biotechnology) according to the manufacturer's instructions. Plates ready for testing were measured by a Biotek Synergy H1 plate reader. Representative results consist of three (or more) independent experiments.

Cellular content fractionation

Cell membranes and cytoplasm were separated using digitonin lysis buffer (25mM Tris-HCl, 150mM NaCl, 0.015% digitonin): first, cells were lysed using digitonin lysis buffer for 10min and centrifuged at 8000 rpm for 2min at 4℃, and the supernatant (cytoplasmic fraction) collected, resuspended in SDS loading buffer, boiled for 5min, used for the SDS-PAGE and Western blotting.

***In vivo* and *in vitro* deubiquitination assay**

For *in vivo* deubiquitination, V5-tagged Ub plasmid and other needed plasmids were transfected in HEK293T cells, and the cells were then treated overnight with 10μM proteasome inhibitor MG132 (Beyotime Biotechnology). These cells were lysed with cell lysis buffer after 48hrs and incubated with a certain amount of α-Flag-agarose overnight at 4℃, and analyze by Western blotting.

For *in vitro* deubiquitination experiments, HEK293T cells were co-transfected with Flag-Axin1 and V5-Ub treated with 10μM MG132 overnight. After 48hrs, cells were lysed and 200μL was left as input, and the remaining whole cell lysate was incubated with a certain amount of Flag beads overnight at 4℃. After binding, the beads were washed with lysis buffer for later use. Meanwhile Myc-USP10 WT and Myc-USP10 CA were expressed in HEK293T cells and purified using α-Myc-agarose. Purified proteins were eluted with 100ng/mL Myc-tag peptide. Eluted USP10 WT or USP10

CA proteins were then incubated with prepared Flag-Axin1 beads in deubiquitination buffer (50mM Tris-HCl, pH 7.4, 1mM $MgCl_2$ and 1mM DTT) for 2hrs at 37°C. The beads (Flag-Axin1) were washed five times by TBS with sufficient shaking during each interval and then analyzed by Western blotting.

Pull-down assay

Preparation of GST fusion protein: Recombinant plasmids with the target gene in pGEX-4T-1 were transformed to *E. coli* BL21 competent cells. Protein expression was induced by addition of IPTG (Beyotime Biotechnology) and shaken at 180rpm for 6-8hrs at 18°C. The bacterial solution was then collected, centrifuged, and the pellet was resuspended in 20 mL of ice lysis buffer (1mM PMSF, Tris, NaCl, and glycerol), and sonicated by SCIENTZ JY92-IIN sonicator on ice at 40% power for 5s each time at 5s intervals for 20min. The bacterial solution after sonication was centrifuged at 4°C for 10min. Transfer the supernatant to a 50mL centrifuge tube. An appropriate amount of GST resins was added to the lysis buffer and incubated for 2-3hrs at 4°C with rotation. The binding beads were washed three times in ice-cold TBS and brought to volume with 1mL TBS (1mM PMSF) for GST-pull down experiments.

GST-pull down: GST-pull down analysis was performed to collect HEK293T cell lysates transferred with the target protein. A small amount of supernatant was obtained as input control, and the remaining lysate was added with beads coupled with GST-fusion expression protein and incubated overnight at 4°C. Beads were washed three times with lysis buffer, the supernatant was aspirated, and an appropriate amount of loading buffer, resuspended in SDS loading buffer, boiled for 5min, used for the SDS-PAGE and Western blotting.

Preparation of His6-tagged protein: The general protocol was the similar with GST-tagged protein preparation. The Ni-NTA resins were used to enrich His6-tagged protein and imidazole was used to elute. Imidazole was removed by dialysis at 4°C overnight.

Whole-mount *in situ* hybridization

911 Digoxigenin-UTP-labeled antisense RNA probes were synthesized in vitro using the
912 MEGAscript Kit (Ambion) according to the manufacturer's instructions. Whole-
913 mount *in situ* hybridization (WISH) with the RNA probes was performed as
914 previously described methods[57].

915 **RNA microinjections**

916 Capped mRNAs were synthesized in vitro for USP10, GFP from the corresponding
917 linearized plasmids using the mMessage mMachine kit (Ambion) according to the
918 manufacturer's instructions. The mRNA was injected into the embryos at 1-cell stage
919 with a concentration of 500ng/μL or co-injected with 100ng/μL ΔN-β-catenin mRNA,
920 1nL per embryo.

921 **Chemical treatments**

922 The USP10 inhibitor, Spautin-1(Beyotime), was dissolved in DMSO with a
923 concentration of 10mM as stock solution. HEK293T were treated with the inhibitor
924 Spautin-1 at a final concentration of 10μM. Embryos were treated with the inhibitor
925 Spautin-1 at a final concentration of 5μM or 10μM (diluted in Holtfreter's solution)
926 form 8-cell stage. Intestinal organoids were treated with the inhibitor Spautin-1 at a
927 final concentration of 20μM, and then harvested at the indicated stage for further
928 analysis.

929 **Mouse intestinal organoids culture**

930 The general process was described in [44]. Freshly isolated mouse crypts or single cells
931 from dissociated mouse intestinal stem cell (ISC) colonies were embedded in Matrigel
932 gels (Corning), which were cast into 20μL droplets at the bottom of wells in 96-well
933 plate. Following polymerization (10min, 37°C), the gels were overlaid with 150μL of
934 ISC expansion medium (Advanced DMEM/F12 containing Glutamax, HEPES,
935 penicillin-streptomycin, B27, N2 (Gibco) ,1μM N-acetylcysteine (Sigma) and 10mM
936 Nicotinamide (Sigma), supplemented with growth factors, including EGF (50ng/mL;
937 Gibco), Wnt, Noggin, R-spondin1 (produced in-house), and small molecules,
938 including CHIR99021 (5μM; Sigma) and Spautin-1 (20μM; Beyotime). The

organoids were infected by lentivirus for 72hrs. The specific protocols were descried in (Bon-Kyoung Koo at al. 2013).

Immunofluorescence analysis

Mouse intestinal organoids embedded in Matrigel gels were fixed with 4% paraformaldehyde (PFA) in PBS (30min, room temperature). The fixation process typically led to complete degradation of the Matrigel. Suspended tissues were collected and centrifuged (800rpm, 5min) to remove the PFA, washed with ultra-pure water and pelleted. Following resuspension in water, the organoids were spread on glass slides and allowed to attach by drying. Attached organoids were rehydrated with PBS. Following fixation, organoids spreaded on glass were permeabilized with 0.2% Triton X-100 in PBS (1h, room temperature) and blocked (10% goat serum in PBS containing 0.01% Triton X-100) for at least 3hrs. Samples were subsequently incubated overnight at 4°C with primary antibodies against Ki67 (1:50; CST #9499) and KRT20 (1:50; ABclonal A17997) diluted in blocking buffer. After washing with PBS for at least 3hrs, samples were incubated 2hrs at 4°C with secondary antibody (1:1000 in blocking solution; Invitrogen). Following extensive washing, stained organoids were imaged in confocal microscope (DM6000CS, Leica).

SW480 (parental or modified) cells were grown on glass coverslips. After growing to 60% confluency, cells were washed three times with PBS and fixed in 4% paraformaldehyde (Sigma), followed by blocking in 5% BSA with 0.2% Triton X-100 for 30min and incubation with primary antibody Axin1 (#2087, 1:200, Cell Signaling Technology) overnight. After that, secondary antibody (A-21429,1:500, Invitrogen) for 40min and nuclei were stained with Hoechst/DAPI (Thermo). Finally, samples were visualized using a confocal fluorescent microscope (DM6000CS, Leica).

***In vitro* droplet formation assays**

Axin1-mCherry, USP10 WT-GFP, USP10 CA-GFP, USP10-ΔDUB-GFP and USP10-ΔDUB-ΔPBR-GFP were transformed into *E. coli* BL21 strand for IPTG-induced expression (see Pull-down assay), followed by GST-resin packed column for purification. Reduced glutathione was used to elute the protein. After overnight

968 dialysis at 4°C, the purified proteins were stored in phase separation buffer (20mM
969 HEPES, 1M NaCl, pH 7.4). NaCl concentration was adjusted to the indicated
970 concentration (150mM, pH 7.4) with buffer containing 20 mM HEPES at the time of
971 used. Mixtures were immediately treated with PEG8000 (Differences in the nature of
972 phase separation between proteins determine the critical concentration at which
973 droplets are formed).10μL of the reaction mixture was prepared; the concentration of
974 NaCl was further adjusted to 150mM NaCl, and the mixture was dropped onto a glass
975 slide and covered with a coverslip at the above concentration, allowed to stand for a
976 few minutes, incubated, and then examined for droplet formation. For imaging,
977 droplets were viewed on glass slides or in glass-bottom cell culture dishes for droplet
978 and fluorescence imaging using ZOE^{TM} Fluorescent Cell Imager (BIO-RAD).

979 **Methyl thiazolyl tetrazolium (MTT) assay for cell proliferation**

980 Cells were seeded on 96-well plates at a density of 1000 cells per well in triplicate,
981 incubated for 1-10 days, and cell density was measured on days 2, 4, 6, 8, and 10 after
982 seeding. At each time point, 10μL of MTT (thiazolyl blue tetrazolium, from Sigma)
983 was added to each well at a final concentration of 0.5mg/mL, and plates were
984 incubated for an additional 4hrs at 37°C. After incubation, all MTT was removed and
985 100μL DMSO was added to each well. Plates ready for testing were measured after 10
986 minutes using a Biotek Synergy H1 plate reader at OD_{490}. Growth curves were plotted
987 on a daily basis based on OD_{490} values. Statistical analysis was done by two-way
988 analysis of variance in Prism 8.0.

989 **Colony formation assay**

990 At a density of 1000 cells /well, the DLD-1 cells were seeded in 6-well plates, and
991 then the cells were cultured in a 37°C incubator for 14 days to allow colony
992 formation. After the size and number of clones grew to a certain extent, the cells were
993 washed and treated with PBS, fixed with 4% paraformaldehyde for 30min, stained
994 with 0.5% crystal violet for 20min, washed with ddH_2O several times and
995 photographed with a digital camera. All assays were performed in triplicate.

996 **Cell migration assays**

Cells were seeded into six-well plates. After reaching 95-100% cell density, 10μL plastic pipette tips were then used to generate scratches in each well. CRC cells were washed with PBS and then maintained in the medium containing 1% FBS. Wound margins were photographed at 0, 24 and 48hrs. Cell migration ability was assessed by measuring the distance between the advancing edges of cells in the microscopic field at each time point. The formula was as follows: 24hrs migration% = (0hr width - 24hrs width of wound)/(0hr width of wound), 48hrs migration% = (0hr width - 48hrs width of wound)/(0hr width of wound). All of the experiments were repeated three times.

Growth of cells in athymic nude mouse and tumor size determination

DLD-1 cells were trypsinized, washed and resuspended in 0.1mL DMEM medium without serum. Eighty 6-week-old female athymic mice (Beijing HFK Biotechnology Co., Ltd.) were randomly divided into 8 groups (10 mice/group), and then the designated cells (1×10^6) were subcutaneously injected into the plate. Tumor size was determined every 2-3 days. Tumor volume was measured, and tumor volume was calculated using each formula: ½ (Length × $Width^2$). Mice were then sacrificed and tumors were excised, weighed and evaluated by immunohistochemistry.

Immunohistochemistry

Mouse immunohistochemistry tissue samples were fixed in 10% formalin, embedded in paraffin, sectioned, deparaffinized, treated with 3% hydrogen peroxide for 10min, submerging in citric acid (pH 6.0) and microwaved for antigen retrieval, and cooled at room temperature (RT) and incubated in normal goat serum for 1hr to block non-specific binding, then incubated with hematoxylin-eosin staining for 10min or overnight at 4℃ using the following primary antibodies: β-catenin (1:200, #8480, Cell Signaling Technology), Ki67 (1:400, #9449, Cell Signaling Technology). The staining was examined using HRP Envision Systems (DAB Kit, MXB Biotechnologies) and analyzed using a dissecting microscope (Leica DM4000).

The human tissue microarrays were purchased from Shanghai Outdo Biotech Company, China. After deparaffinizing in xylene and rehydrating in graded ethanol,

tissue microarrays were immersed in citrate buffer (USP10, Axin1) or EDTA (β-catenin) for antigen retrieval. Endogenous peroxidase was quenched using 3% hydrogen peroxide for 30min. To decrease the nonspecific staining, 10% normal goat serum was subsequently used to block tissue collagen for 30min. Tissue sections were then incubated with antibody anti-USP10 (#8501, 1:100, Cell Signaling Technology), anti-Axin1 (#2087, 1:100, Cell Signaling Technology) or anti-β-catenin (sc-7963, 1:500, Sigma) for 90min at room temperature (24-27°C) at 4°C overnight. After that, biotinylated secondary antibody and streptavidin-biotin peroxidase were used to incubate tissue sections for 10min each in turn. Slides were stained with DAB chromogenic reagent for 60s, afterwards counterstained with hematoxylin. UltraSensitiveTM SPIHC Kit (KIT-9720, Maixin Inc., Fujian, China) were used in this experiment.

The stained sections were reviewed and scored by two investigators independently and the different scoring was resolved after discussion. We adopted a semi-quantitative scoring method to assess the expression of certain protein. The staining intensity was divided into 0 (no staining), 1 (weak staining), 2 (moderate) and 3 (strong). The percentage of cells stained was categorized as 0 (0-5%), 1 (6-25%), 2 (26-50%), 3 (51-75%), and 4 (76%-100%). The final scores were generated by multiplying the staining intensity by percentage of cells.

Confocal laser scanning microscopy

All plasmid transfection fluorescence images were conducted on Olympus spinning disk confocal microscope with an IX83 fully motorized inverted microscope and a 100XO UPLSAPO oil lens (numerical aperture 1.42) (Olympus). mCherry was excited at 594 nm and detected at 610-710nm.

Fluorescence recovery after photobleaching (FRAP) experiments

Cells were firstly transfected with the plasmids of interest. After 2 days of transfection and expression of the target proteins, the FRAP experiments of these cells were conducted using a Fluoview FV3000 confocal laser scanning microscope with a 100XO UPLSAPO oil lens (numerical aperture 1.4) (Olympus). A condensate of the

proteins of interests or a small region of the condensate was selected and bleached using a 594nm argon laser at 100% intensity in five repeats with a dwell time of 50ms. Time-lapse images were recorded with an internal of 0.09ms between each frame. FRAP analysis was completed using the ImageJ FRAP Profiler plugin (from the Hardin lab: https://worms.zoology.wisc.edu/research/4d/4d.html#frap). The mobile fraction (f_m) and the immobile fraction (f_i) was calculated by the following equations:

$f_m = F_\infty / F_0$

where F_∞ is the fluorescence intensity after full recovery, and F_0 is the fluorescence intensity before photobleaching.

$f_i = 1 - f_m$

FRAP curve was plotted with Prism 8 software, and $t_{1/2}$ was calculated by fitting the curve with exponential decay function.

Quantification and statistical analysis

P-values were determined with Student's t-test, One-way or Two-way ANOVA with post hoc Tukey's HSD test between comparator groups using GraphPad Prism software based on the individual mathematic model of each data set.

WB stripe quantification was performed by Image J:

Using Image J→ Analyze→Gels→Plot Lanes to analyze the Western Blot results.

If statistical analysis is required, three independent experiments were performed and quantified. Unpaired two-tailed Student's t-test was used to determine statistical significance.

For the quantification of Axin1 puncta *in vitro*, maximum projections of 10 z-stack images (0.9μm apart) were manually generated. For the quantification of Axin1 puncta *in vivo*, all images presented in the paper were z-stack maximum projections using a step size of 0.27μm, spanning the entire depth of the nucleus. Puncta number and diameter were analyzed using the software ImageJ. Unpaired two-tailed Student's t-test was used to determine statistical significance.

TOPFlash assay: After the values were obtained according to the TOPFlash Dual-luciferase reporter assay method, the fluorescence values of Firefly were divided by the corresponding fluorescence values of Renilla (internal control). The values of EV + LCM were used as control, and all the values were divided by the values of EV + LCM for normalization, and the obtained results were used for image drawing. Experimental results are shown as the mean ± SD, n=3 replicates, one-way ANOVA or two-tailed Student's t-test was performed for statistical analysis.

MTT assay: The OD_{490} values at each time point was used as the result for image drawing. Experimental results are shown as the mean ± SD, n=3 replicates, two-way ANOVA was performed for statistical analysis.

Quantitative real-time PCR: The gene expression values were normalized to those of GAPDH. And data processing was performed using the $2^{-\Delta\Delta Ct}$ method, the results were calculated for image drawing. Experimental results are shown as the mean ± SD, n=3 replicates, two-tailed Student's t-test was performed for statistical analysis.

Tumor volumes: Tumor volume was calculated using the formula: ½ (Length × $Width^2$). Images were drawn after obtaining the tumor volumes in combination with the corresponding time points. Experimental results are shown as the mean ± SD, n=10 for each group, two-way ANOVA was performed for statistical analysis.

Tumor weight: The tumor weight was measured after sacrificing the nude mice and dissecting the tumor. Images were drawn based on the weight results. Experimental results are shown as the mean ± SD, n=10 for each group, two-tailed Student's t-test was performed for statistical analysis.

Endogenous Axin1 puncta in SW480 cells: each group selects three different visual fields (25um), and counts the cells through ImageJ. Experimental results are shown as the mean ± SD, and n was labelled within the figures. Unpaired two-tailed Student's t-test was used to determine statistical significance.

In vitro droplet formation: puncta number and diameter of Axin1 were analyzed using the software ImageJ. Experimental results are shown as the mean ± SD, and n was

labelled within the figures. Unpaired two-tailed Student's t-test was used to determine statistical significance.

Colony number: Image J→ Type:8-bit→Adjust:Threshold→Analyze:Analyze Particles to analyze the colony formation results[58]. Experimental results are shown as the mean ± SD. Unpaired two-tailed Student's t-test was used to determine statistical significance.

Reference

1 MacDonald, B. T., Tamai, K. & He, X. Wnt/beta-catenin signaling: components, mechanisms, and diseases. *Developmental cell* **17**, 9-26, doi:10.1016/j.devcel.2009.06.016 (2009).

2 Nusse, R. & Clevers, H. Wnt/beta-Catenin Signaling, Disease, and Emerging Therapeutic Modalities. *Cell* **169**, 985-999, doi:10.1016/j.cell.2017.05.016 (2017).

3 Storm, E. E. *et al.* Targeting PTPRK-RSPO3 colon tumours promotes differentiation and loss of stem-cell function. *Nature* **529**, 97-100, doi:10.1038/nature16466 (2016).

4 Bendell, J. *et al.* Initial results from a phase 1a/b study of OMP-131R10, a first-in-class anti-RSPO3 antibody, in advanced solid tumors and previously treated metastatic colorectal cancer (CRC). *Eur J Cancer* **69**, S29-S30, doi:Doi 10.1016/S0959-8049(16)32668-5 (2016).

5 Chartier, C. *et al.* Therapeutic Targeting of Tumor-Derived R-Spondin Attenuates beta-Catenin Signaling and Tumorigenesis in Multiple Cancer Types. *Cancer research* **76**, 713-723, doi:10.1158/0008-5472.CAN-15-0561 (2016).

6 Kakugawa, S. *et al.* Notum deacylates Wnt proteins to suppress signalling activity. *Nature* **519**, 187-192, doi:10.1038/nature14259 (2015).

7 Zhang, X. *et al.* Notum is required for neural and head induction via Wnt deacylation, oxidation, and inactivation. *Developmental cell* **32**, 719-730, doi:10.1016/j.devcel.2015.02.014 (2015).

8 Flanagan, D. J. *et al.* NOTUM from Apc-mutant cells biases clonal competition to initiate cancer. *Nature* **594**, 430-435, doi:10.1038/s41586-021-03525-z (2021).

9 Ter Steege, E. J. & Bakker, E. R. M. The role of R-spondin proteins in cancer biology. *Oncogene* **40**, 6469-6478, doi:10.1038/s41388-021-02059-y (2021).

10 Nong, J. *et al.* Phase separation of Axin organizes the beta-catenin destruction complex. *The Journal of cell biology* **220**, doi:10.1083/jcb.202012112 (2021).

11 Kim, S. E. *et al.* Wnt stabilization of beta-catenin reveals principles for morphogen receptor-scaffold assemblies. *Science* **340**, 867-870, doi:10.1126/science.1232389 (2013).

12 Huang, S. M. *et al.* Tankyrase inhibition stabilizes axin and antagonizes Wnt signalling. *Nature* **461**, 614-620, doi:10.1038/nature08356 (2009).

13 Zhang, Y. *et al.* RNF146 is a poly(ADP-ribose)-directed E3 ligase that regulates axin degradation and Wnt signalling. *Nature cell biology* **13**, 623-629, doi:10.1038/ncb2222 (2011).

14 Callow, M. G. *et al.* Ubiquitin ligase RNF146 regulates tankyrase and Axin to promote Wnt signaling. *PloS one* **6**, e22595, doi:10.1371/journal.pone.0022595 (2011).

15 Ji, L. *et al.* USP7 inhibits Wnt/beta-catenin signaling through promoting stabilization of Axin. *Nature communications* **10**, doi:ARTN 4184 10.1038/s41467-019-12143-3 (2019).

16 Ji, L. *et al.* The SIAH E3 ubiquitin ligases promote Wnt/beta-catenin signaling through mediating Wnt-induced Axin degradation. *Genes Dev* **31**, 904-915, doi:10.1101/gad.300053.117 (2017).

17 Lui, T. T. *et al.* The ubiquitin-specific protease USP34 regulates axin stability and Wnt/beta-catenin signaling. *Molecular and cellular biology* **31**, 2053-2065, doi:10.1128/MCB.01094-10 (2011).

18 Cha, B. *et al.* Methylation by protein arginine methyltransferase 1 increases stability of Axin, a negative regulator of Wnt signaling. *Oncogene* **30**, 2379-2389, doi:10.1038/onc.2010.610 (2011).

19 Kim, S. & Jho, E. H. The protein stability of Axin, a negative regulator of Wnt signaling, is regulated by Smad ubiquitination regulatory factor 2 (Smurf2). *The Journal of biological chemistry* **285**, 36420-36426, doi:10.1074/jbc.M110.137471 (2010).

20 Swatek, K. N. & Komander, D. Ubiquitin modifications. *Cell research* **26**, 399-422, doi:10.1038/cr.2016.39 (2016).

21 Bhattacharya, U., Neizer-Ashun, F., Mukherjee, P. & Bhattacharya, R. When the chains do not break: the role of USP10 in physiology and pathology. *Cell Death Dis* **11**, 1033, doi:10.1038/s41419-020-03246-7 (2020).

22 Weisberg, E. L. *et al.* Inhibition of USP10 induces degradation of oncogenic FLT3. *Nature chemical biology* **13**, 1207-1215, doi:10.1038/nchembio.2486 (2017).

23 Sun, J. *et al.* USP10 inhibits lung cancer cell growth and invasion by upregulating PTEN. *Mol Cell Biochem* **441**, 1-7, doi:10.1007/s11010-017-3170-2 (2018).

24 Lu, C. *et al.* USP10 suppresses tumor progression by inhibiting mTOR activation in hepatocellular carcinoma. *Cancer letters* **436**, 139-148, doi:10.1016/j.canlet.2018.07.032 (2018).

25 Zhu, H. *et al.* USP10 Promotes Proliferation of Hepatocellular Carcinoma by Deubiquitinating and Stabilizing YAP/TAZ. *Cancer research* **80**, 2204-2216, doi:10.1158/0008-5472.CAN-19-2388 (2020).

26 Yuan, J., Luo, K., Zhang, L., Cheville, J. C. & Lou, Z. USP10 regulates p53 localization and stability by deubiquitinating p53. *Cell* **140**, 384-396, doi:10.1016/j.cell.2009.12.032 (2010).

27 Liu, J. *et al.* Beclin1 controls the levels of p53 by regulating the deubiquitination activity of USP10 and USP13. *Cell* **147**, 223-234, doi:10.1016/j.cell.2011.08.037 (2011).

28 Deng, M. *et al.* Deubiquitination and Activation of AMPK by USP10. *Molecular cell* **61**, 614-624, doi:10.1016/j.molcel.2016.01.010 (2016).

29 Lim, R. *et al.* Deubiquitinase USP10 regulates Notch signaling in the endothelium. *Science* **364**, 188-+, doi:10.1126/science.aat0778 (2019).

30 Liao, Y. *et al.* Inhibition of EGFR signaling with Spautin-1 represents a novel therapeutics for prostate cancer. *J Exp Clin Cancer Res* **38**, 157, doi:10.1186/s13046-019-1165-4 (2019).

31 Novellasdemunt, L. *et al.* USP7 Is a Tumor-Specific WNT Activator for APC-Mutated Colorectal Cancer by Mediating beta-Catenin Deubiquitination. *Cell reports* **21**, 612-627, doi:10.1016/j.celrep.2017.09.072 (2017).

32 Tanneberger, K. *et al.* Structural and functional characterization of the Wnt inhibitor APC membrane recruitment 1 (Amer1). *The Journal of biological chemistry* **286**, 19204-19214, doi:10.1074/jbc.M111.224881 (2011).

33 Rivera, M. N. *et al.* An X chromosome gene, WTX, is commonly inactivated in Wilms tumor. *Science* **315**, 642-645, doi:10.1126/science.1137509 (2007).

34 Major, M. B. *et al.* Wilms tumor suppressor WTX negatively regulates WNT/beta-catenin signaling. *Science* **316**, 1043-1046, doi:10.1126/science/1141515 (2007).

35 Tiwary, A. K. & Zheng, Y. X. Protein phase separation in mitosis. *Current Opinion in Cell Biology* **60**, 92-98, doi:10.1016/j.ceb.2019.04.011 (2019).

36 Davis, R. B., Moosa, M. M. & Banerjee, P. R. Ectopic biomolecular phase transitions: fusion proteins in cancer pathologies. *Trends Cell Biol* **32**, 681-695, doi:10.1016/j.tcb.2022.03.005 (2022).

37 Banani, S. F., Lee, H. O., Hyman, A. A. & Rosen, M. K. Biomolecular condensates: organizers of cellular biochemistry. *Nat Rev Mol Cell Bio* **18**, 285-298, doi:10.1038/nrm.2017.7 (2017).

38 Li, Y. *et al.* Volumetric Compression Induces Intracellular Crowding to Control Intestinal Organoid Growth via Wnt/beta-Catenin Signaling. *Cell Stem Cell* **28**, 63-78 e67, doi:10.1016/j.stem.2020.09.012 (2021).

39 Martino-Echarri, E., Brocardo, M. G., Mills, K. M. & Henderson, B. R. Tankyrase Inhibitors Stimulate the Ability of Tankyrases to Bind Axin and Drive Assembly of beta-Catenin Degradation-Competent Axin Puncta. *PloS one* **11**, e0150484, doi:10.1371/journal.pone.0150484 (2016).

40 Schneider, S., Steinbeisser, H., Warga, R. M. & Hausen, P. beta-Catenin translocation into nuclei demarcates the dorsalizing centers in frog and fish embryos. *Mech Develop* **57**, 191-198, doi:Doi 10.1016/0925-4773(96)00546-1 (1996).

41 Parker, D. S., Ni, Y. Y., Chang, J. L., Li, J. & Cadigan, K. M. Wingless signaling induces widespread chromatin remodeling of target loci. *Molecular and cellular biology* **28**, 1815-1828, doi:10.1128/MCB.01230-07 (2008).

42 Kelly, C., Chin, A. J., Leatherman, J. L., Kozlowski, D. J. & Weinberg, E. S. Maternally controlled beta-catenin-mediated signaling is required for organizer formation in the zebrafish. *Development* **127**, 3899-3911 (2000).

43 Dorsky, R. I., Sheldahl, L. C. & Moon, R. T. A transgenic Lef1/beta-catenin-dependent reporter is expressed in spatially restricted domains throughout zebrafish development. *Dev Biol* **241**, 229-237, doi:10.1006/dbio.2001.0515 (2002).

44 Sato, T. *et al.* Single Lgr5 stem cells build crypt-villus structures in vitro without a mesenchymal niche. *Nature* **459**, 262-265, doi:10.1038/nature07935 (2009).

45 Almeqdadi, M., Mana, M. D., Roper, J. & Yilmaz, O. H. Gut organoids: mini-tissues in culture to study intestinal physiology and disease. *Am J Physiol Cell Physiol* **317**, C405-C419, doi:10.1152/ajpcell.00300.2017 (2019).

46 Sato, T. & Clevers, H. Growing self-organizing mini-guts from a single intestinal stem cell: mechanism and applications. *Science* **340**, 1190-1194, doi:10.1126/science.1234852 (2013).

47 Zhan, T., Rindtorff, N. & Boutros, M. Wnt signaling in cancer. *Oncogene* **36**, 1461-1473, doi:10.1038/onc.2016.304 (2017).

48 Koo, B. K. *et al.* Tumour suppressor RNF43 is a stem-cell E3 ligase that induces endocytosis of Wnt receptors. *Nature* **488**, 665-669, doi:10.1038/nature11308 (2012).

49 Giannakis, M. *et al.* RNF43 is frequently mutated in colorectal and endometrial cancers. *Nat Genet* **46**, 1264-1266, doi:10.1038/ng.3127 (2014).

50 Seshagiri, S. *et al.* Recurrent R-spondin fusions in colon cancer. *Nature* **488**, 660-664, doi:10.1038/nature11282 (2012).

51 He, Y. *et al.* The deubiquitinase USP10 restores PTEN activity and inhibits non-small cell lung cancer cell proliferation. *The Journal of biological chemistry* **297**, 101088, doi:10.1016/j.jbc.2021.101088 (2021).

52 Kim, K. *et al.* Prognostic significance of USP10 and p14ARF expression in patients with colorectal cancer. *Pathol Res Pract* **216**, 152988, doi:10.1016/j.prp.2020.152988 (2020).

53 Wang, X. *et al.* The deubiquitinase USP10 regulates KLF4 stability and suppresses lung tumorigenesis. *Cell Death Differ* **27**, 1747-1764, doi:10.1038/s41418-019-0458-7 (2020).

54 Dennler, S. *et al.* Direct binding of Smad3 and Smad4 to critical TGF beta-inducible elements in the promoter of human plasminogen activator inhibitor-type 1 gene. *EMBO J* **17**, 3091-3100, doi:10.1093/emboj/17.11.3091 (1998).

55 Schneider, C. A., Rasband, W. S. & Eliceiri, K. W. NIH Image to ImageJ: 25 years of image analysis. *Nat Methods* **9**, 671-675, doi:10.1038/nmeth.2089 (2012).

56 Kimmel, C. B., Ballard, W. W., Kimmel, S. R., Ullmann, B. & Schilling, T. F. Stages of embryonic development of the zebrafish. *Developmental dynamics : an official publication of the American Association of Anatomists* **203**, 253-310, doi:10.1002/aja.1002030302 (1995).

57 Wei, S. *et al.* The guanine nucleotide exchange factor Net1 facilitates the specification of dorsal cell fates in zebrafish embryos by promoting maternal beta-catenin activation. *Cell Res* **27**, 202-225, doi:10.1038/cr.2016.141 (2017).

58 Cai, Z. L. *et al.* Optimized digital counting colonies of clonogenic assays using ImageJ software and customized macros: Comparison with manual counting. *Int J Radiat Biol* **87**, 1135-1146, doi:10.3109/09553002.2011.622033 (2011).

Supplementary Information

Supplementary figure legends

Supplementary Figure 1. Additional experimental results demonstrate USP10 inhibits Wnt/β-catenin signaling.

(a) TOPFlash reporter assay showing USP10 inhibits Wnt/β-catenin signaling in HEK293T cell. Axin1 is used as positive control. Error bars mean ± SD, n = 3, two-tailed Student's t-test.

(b) TOPFlash reporter assay showing USP10 inhibits Wnt/β-catenin signaling in RKO cell. Axin1 is used as positive control. Error bars mean ± SD, n = 3, two-tailed Student's t-test.

(c) TOPFlash reporter assay showing USP10 inhibits Wnt/β-catenin signaling in DLD-1 cell in the absence of exogenous Wnt. Axin1 is used as positive control. Error bars mean ± SD, n = 3, two-tailed Student's t-test.

(d) Sanger sequence of the two clones of USP10 CRISPR-Cas9 knockout in HEK293T cells.

(e) Validation of USP10 knockout by WB.

(f) Validation of USP10 shRNA knockdown by RT-qPCR and WB. Error bars mean ± SD, n = 3, two-tailed Student's t-test. shUSP10-1 was used and abbreviated as shUSP10 in sequel experiments.

(g) Knockdown of USP10 significantly enhances TOPFlash reporter at the presence of Wnt3a CM. Error bars mean ± SD, n = 3, two-tailed Student's t-test.

(h) WB assay showing the alteration of cytosolic β-catenin levels under USP10 overexpression or knockdown condition.

(i) Dual-luciferase chemiluminescence of ARE, BRE, CAGA, TCF, SRE and CRE under control CM or Wnt3a CM treatment. Error bars mean ± SD, n = 3, two-tailed Student's t-test.

(j) WB assay showing USP10 overexpression cannot effectively reduce the cytosolic ΔN-β-catenin level.

RLU: Relative Luciferase Unit. ns, not significant.

Supplementary Figure 2. Supportive information for deubiquitination and stabilization of Axin1 by USP10.

(a) Co-IP of USP10 with exogenous key components of β-catenin destruction complex, including Axin1, β-Trcp, β-catenin, GSK3 and APC.

(b) Validation of USP10 knockdown effect on AXIN1 and CTNNB1 transcription levels. Error bars mean ± SD, n = 3, two-tailed Student's t-test.

(c) WB showing endogenous Axin1 level increases with USP10 dose-dependently.

(d) Quantifications of Axin1 levels in the pulse-chase assay shown by Figure 2c.

(e) Pulse-chase assay of endogenous Axin1 under USP10 KO conditions.

(f) Validation of human Axin1 knockdown by RT-qPCR. shAxin1-1 was used and abbreviated as shAxin1 in sequel experiments. Error bars mean ± SD, n = 3, two-tailed Student's t-test.

(g) Ubiquitination assay of Axin1 under USP10 knockout and rescue conditions.

(h) *In vitro* deubiquitination assay of USP10 on Axin1.

(i) Ubiquitination assay showing USP10-CA mutant loses the capability to deubiquitinate exogenous Axin1.

(j) Ubiquitination assay showing USP10 does not deubiquitinate β-catenin.

(k) Pulse-chase assay of endogenous Axin1 under Spautin-1 treatment.

(l) TOPFlash reporter assay in parental or USP10 KO HEK293T cell under Spautin-1 treatment. Error bars mean ± SD, n = 3, two-tailed Student's t-test.

Supplementary Figure 3. Supportive information for Axin1 and USP10 binding study.

(a) *In vitro* pull-down assay of bacterial expressed Axin1 and USP10. Asterisks represent the major bands of the desired proteins.

(b) Co-IP assay of different segments of USP10 with Axin1.

(c) Amino acid sequence alignment showing the seven conserved regions on ΔDUB of vertebrate USP10.

(d) Pull-down assay of Axin1 with different conserved regions of USP10-ΔDUB. Asterisks represent the major bands of the desired proteins.

(e) Schematic drawing of Axin1 protein. N, N-terminal; RGS, RGS domain; GSK3, GSK3 binding helix; β-cat, β-catenin binding site; CK1, CK1 putative binding site; DIX, DIX domain.

(f) Pull-down assay of USP10 with different regions of Axin1. Asterisks represent the major bands of the desired proteins.

(g) Axin1 WT/DA levels alterations under USP10 WT or ΔPBR overexpression condition.

Supplementary Figure 4. Supportive information showing USP10 physically mediate Axin1 and β-catenin interaction.

(a) Ubiquitination assay of Axin1 under USP10 WT, CA, and ΔDUB overexpression.

(b) WB assay showing cytosolic β-catenin level diminishes dose-dependently of USP10-ΔDUB.

(c) *In vitro* pull-down assay of bacterial expressed β-catenin and USP10. Asterisks represent the major bands of the desired proteins.

(d) Pull-down assay showing different segments of USP10 interacting with β-catenin.

(e, f) Co-IP assay of USP10 ΔDUB with different segments of β-catenin.

(g) Co-IP assay showing depletion of USP10 results in the reduced interaction between endogenous Axin1 and β-catenin.

(h) TOPFlash reporter assay showing USP10 ΔS2+DUBCA and USP10 S2+S3+DUBCA behave dominant-negatively. Error bars mean ± SD, n = 3, two-tailed Student's t-test.

RLU: Relative Luciferase Unit. ns, not significant.

Supplementary Figure 5. Supportive information showing USP10 promotes Axin1 granule formation.

(a) Representative fluorescent images showing the fusion of Axin1 puncta.

(b) Representative images of the FRAP assay of Axin1 puncta.

(c) Recovery of fluorescent intensity after the photobleaching during the FRAP assay of Axin1 puncta.

(d) Sanger sequence of the USP10 CRISPR-Cas9 knockout in SW480 cells.

(e) Protein level validation of USP10 KO and rescue in SW480 in Figure 4h.

(f) Representative fluorescent images of Axin1 droplets (WT and DA).

(g, h) Numbers of Axin1 puncta per cell (g), size of Axin1 puncta (h). Error bars mean ± SD, two-tailed Student's t-test.

Supplementary Figure 6. Supportive assays of zebrafish embryo study.

(a) Expression analysis of the zebrafish *usp10* transcript at the indicated stages by whole-mount *in situ* hybridization. Embryos were shown with lateral view except the 16-cell stage (animal pole views).

(b-e) USP10 promoted the stabilization of Axin1. The hUSP10 overexpression and Spautin-1 treated embryos were collected at sphere stage for WB with the indicated antibodies (b and d) and the protein levels were analyzed respectively in (c and e). Error bars mean ± SD, n = 3, two-tailed Student's t-test.

Supplementary Figure 7. Supportive assays of intestinal organoid study.

(a) Validation of murine USP10 knockdown by WB. shUSP10-1 was used and abbreviated as shUSP10 in the sequel experiments.

(b) WB showing USP10 and Axin1 levels under USP10 depletion and/or XAV939 treatment.

(c) Percentage of sphere-like and budded organoids under Spautin-1 and CHIR99021 treatments. DMSO group:n=45, Spautin-1 group:n=46, CHIR99021 group:n=49.

(d) WB assay showing treatment of Spautin-1 effectively reduced endogenous Axin1 level in murine intestinal organoids. shUSP10 was used as control to confirm the effect of Spautin-1.

(e) Representative images of murine intestinal organoids under DMSO, Spautin-1 or CHIR99021 treatment at different doses. All images in the panel are in the same scale.

(f, g) Percentage of sphere-like and budded organoids under Spautin-1 and CHIR99021 treatments.

(h, i) Organoid (sphere-like) diameters quantifications in (e) shown by histogram. Error bars mean ± SD, by two-tailed Student's t-test.

Supplementary Figure 8. Additional assays and information to illustrate the tumor-suppressive effect of USP10 in human CRC.

(a) Endogenous Axin1 and cytosolic β-catenin levels in SW480 cell lines under USP10 Knockout condition.

(b) MTT assay showing USP10 KO significantly enhanced SW480 cell growth. Error bars mean ± SD, n = 3, two-way ANOVA.

(c) Wound healing assay of DLD-1 cell after expression of USP10 WT and USP10-CA. Error bars mean ± SD, n = 3, two-tailed Student's t-test.

(d) MTT cell growth assay of DLD-1 and SW480 cells with the overexpression of dominant negative USP10 mutants. Error bars mean ± SD, n = 3, two-way ANOVA.

(e, f) Quantifications of the numbers of colonies in Figure 7f and 7g. Error bars mean ± SD, by two-tailed Student's t-test.

(g) Images of the tumors formed by subcutaneously transplanted DLD-1 cells after abscission.

(h) Overall survival of USP10-high and -low patients from TCGA-COADREAD database.

(i, j) Correlation analysis between Axin1 and nuclear localized β-catenin ratio based on grouped USP10 levels. Error bars mean ± SD, n = 3, two-tailed Student's t-test. ns, not significant.

Figure 1

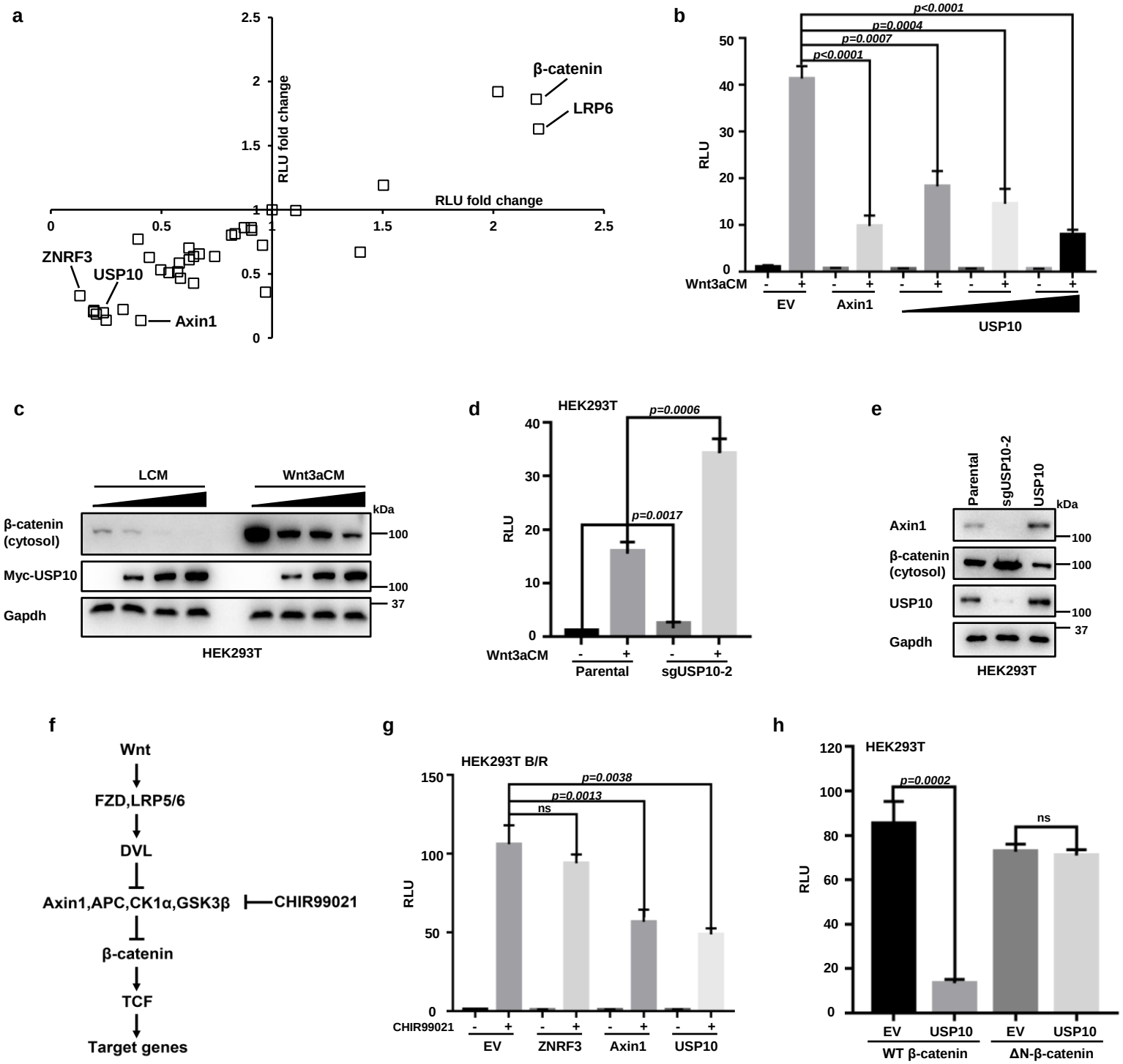
a
RLU fold change
RLU fold change
β-catenin
LRP6
ZNRF3
USP10
Axin1
b
HEK293T B/R
p<0.0001
p=0.0004
p=0.0007
p<0.0001
RLU
Wnt3aCM
EV
Axin1
USP10
c
LCM
Wnt3aCM
kDa
β-catenin (cytosol)
Myc-USP10
Gapdh
HEK293T
d
HEK293T
p=0.0006
p=0.0017
RLU
Wnt3aCM
Parental
sgUSP10-2
e
Parental
sgUSP10-2
USP10
kDa
Axin1
β-catenin (cytosol)
USP10
Gapdh
HEK293T
f
Wnt
FZD,LRP5/6
DVL
Axin1,APC,CK1α,GSK3β
CHIR99021
β-catenin
TCF
Target genes
g
HEK293T B/R
p=0.0038
p=0.0013
ns
RLU
CHIR99021
EV
ZNRF3
Axin1
USP10
h
HEK293T
p=0.0002
ns
RLU
EV
USP10
EV
USP10
WT β-catenin
ΔN-β-catenin

Figure 2

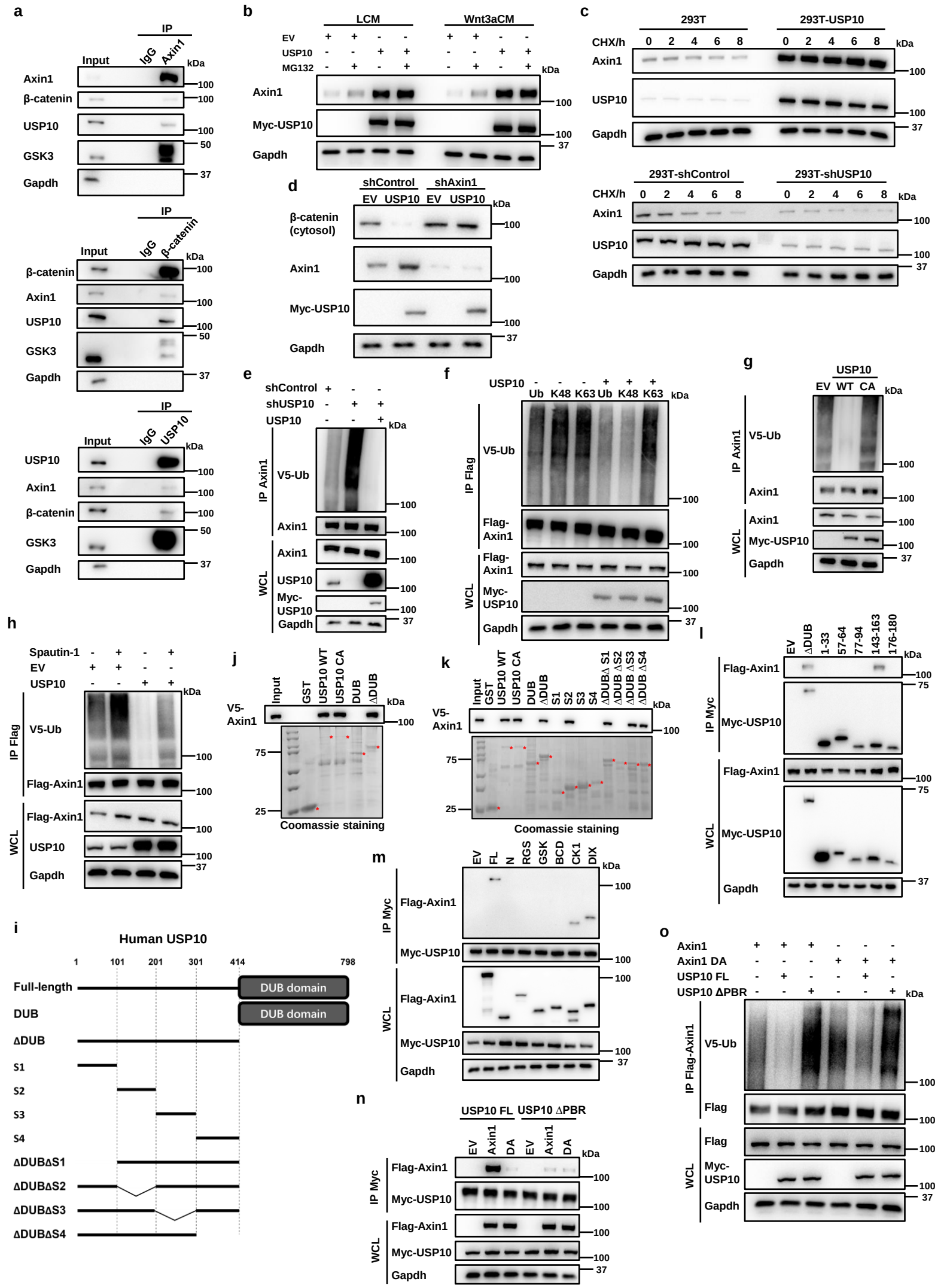
a
IP
Input
IgG
Axin1
kDa
Axin1
β-catenin
USP10
GSK3
Gapdh
100
50
37
IP
Input
IgG
β-catenin
β-catenin
Axin1
USP10
GSK3
Gapdh
IP
Input
IgG
USP10
USP10
Axin1
β-catenin
GSK3
Gapdh
b
LCM
Wnt3aCM
EV
USP10
MG132
Axin1
Myc-USP10
Gapdh
c
293T
293T-USP10
CHX/h
0 2 4 6 8
Axin1
USP10
Gapdh
293T-shControl
293T-shUSP10
d
shControl
shAxin1
EV USP10 EV USP10
β-catenin (cytosol)
Axin1
Myc-USP10
Gapdh
e
shControl
shUSP10
USP10
IP Axin1
V5-Ub
Axin1
WCL
Axin1
USP10
Myc-USP10
Gapdh
f
USP10
Ub K48 K63 Ub K48 K63
IP Flag
V5-Ub
Flag-Axin1
WCL
Flag-Axin1
Myc-USP10
Gapdh
g
USP10
EV WT CA
IP Axin1
V5-Ub
Axin1
WCL
Axin1
Myc-USP10
Gapdh
h
Spautin-1
EV
USP10
IP Flag
V5-Ub
Flag-Axin1
WCL
Flag-Axin1
USP10
Gapdh
j
Input
GST
USP10 WT
USP10 CA
DUB
ΔDUB
V5-Axin1
75
25
Coomassie staining
k
Input
GST
USP10 WT
USP10 CA
DUB
ΔDUB
S1
S2
S3
S4
ΔDUBΔ S1
ΔDUB ΔS2
ΔDUB ΔS3
ΔDUB ΔS4
V5-Axin1
75
25
Coomassie staining
l
EV
ΔDUB
1-33
57-64
77-94
143-163
176-180
IP Myc
Flag-Axin1
Myc-USP10
WCL
Flag-Axin1
Myc-USP10
Gapdh
i
Human USP10
1
101
201
301
414
798
Full-length
DUB
ΔDUB
S1
S2
S3
S4
ΔDUBΔS1
ΔDUBΔS2
ΔDUBΔS3
ΔDUBΔS4
DUB domain
DUB domain
m
EV
FL
N
RGS
GSK
BCD
CK1
DIX
IP Myc
Flag-Axin1
Myc-USP10
WCL
Flag-Axin1
Myc-USP10
Gapdh
n
USP10 FL
USP10 ΔPBR
EV
Axin1
DA
IP Myc
Flag-Axin1
Myc-USP10
WCL
Flag-Axin1
Myc-USP10
Gapdh
o
Axin1
Axin1 DA
USP10 FL
USP10 ΔPBR
IP Flag-Axin1
V5-Ub
Flag
WCL
Flag
Myc-USP10
Gapdh

Figure 3

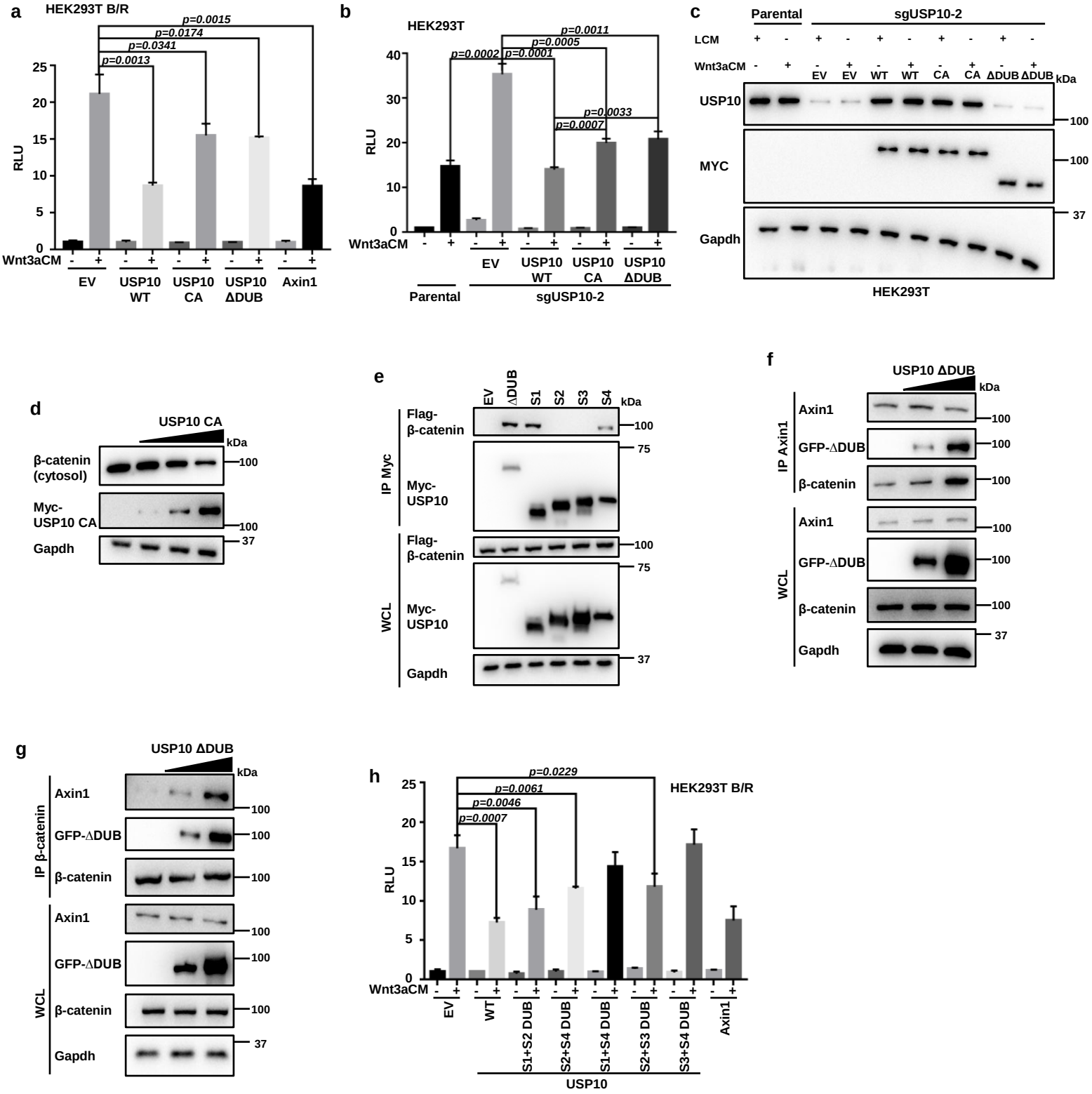
a
HEK293T B/R
p=0.0015
p=0.0174
p=0.0341
p=0.0013
RLU
Wnt3aCM
EV
USP10 WT
USP10 CA
USP10 ΔDUB
Axin1
b
HEK293T
p=0.0011
p=0.0005
p=0.0002
p=0.0001
p=0.0033
p=0.0007
RLU
Wnt3aCM
EV
USP10 WT
USP10 CA
USP10 ΔDUB
Parental
sgUSP10-2
c
Parental
sgUSP10-2
LCM
Wnt3aCM
EV EV WT WT CA CA ΔDUB ΔDUB
kDa
USP10
MYC
Gapdh
100
100
37
HEK293T
d
USP10 CA
kDa
β-catenin (cytosol)
Myc-USP10 CA
Gapdh
100
100
37
e
EV
ΔDUB
S1
S2
S3
S4
kDa
IP Myc
Flag-β-catenin
Myc-USP10
WCL
Flag-β-catenin
Myc-USP10
Gapdh
100
75
100
75
37
f
USP10 ΔDUB
kDa
IP Axin1
Axin1
GFP-ΔDUB
β-catenin
WCL
Axin1
GFP-ΔDUB
β-catenin
Gapdh
100
100
100
100
100
100
37
g
USP10 ΔDUB
kDa
IP β-catenin
Axin1
GFP-ΔDUB
β-catenin
WCL
Axin1
GFP-ΔDUB
β-catenin
Gapdh
100
100
100
100
100
100
37
h
p=0.0229
p=0.0061
p=0.0046
p=0.0007
HEK293T B/R
RLU
Wnt3aCM
EV
WT
S1+S2 DUB
S2+S4 DUB
S1+S4 DUB
S2+S3 DUB
S3+S4 DUB
Axin1
USP10

Figure 4

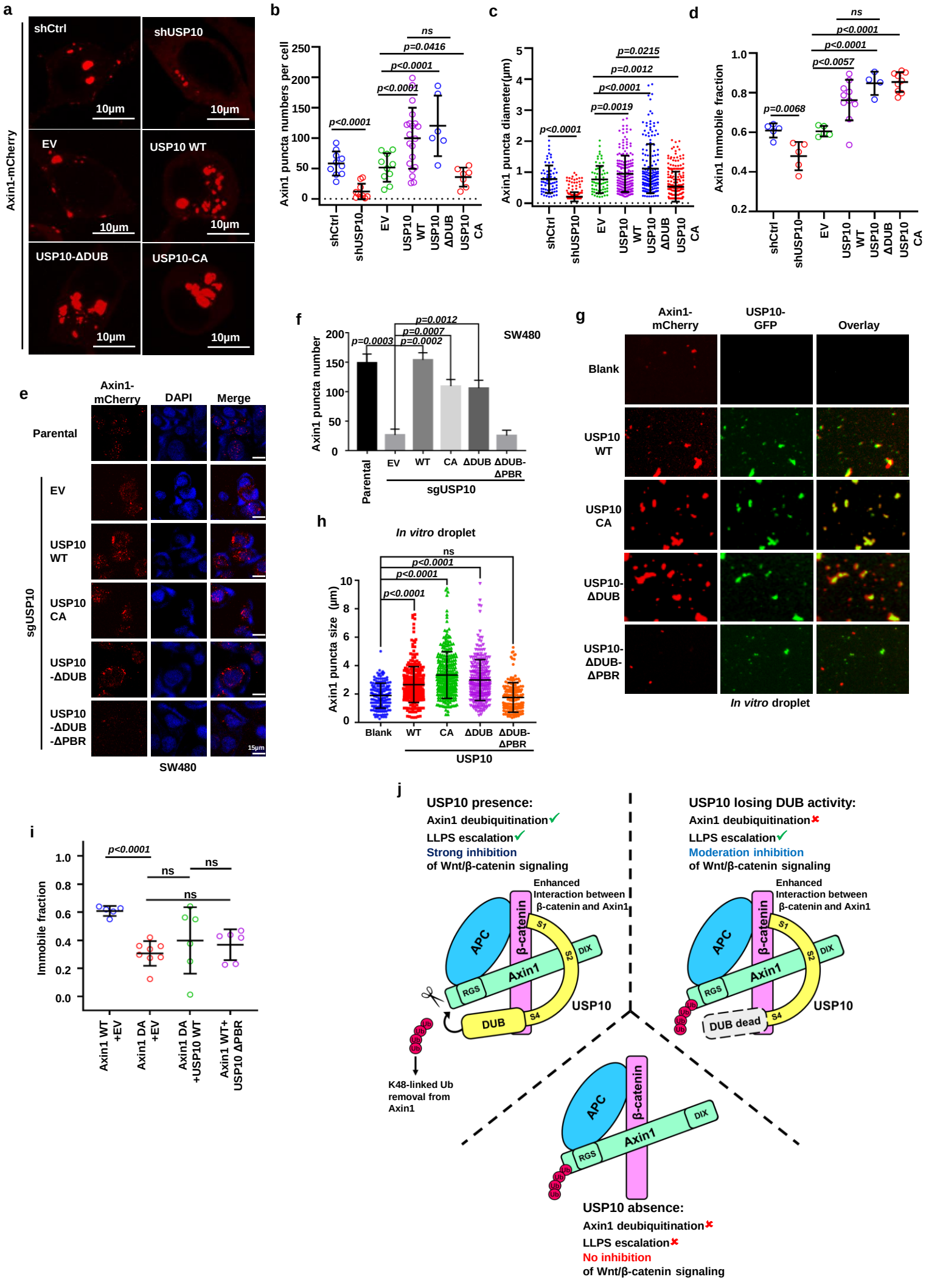
a
Axin1-mCherry
shCtrl
shUSP10
EV
USP10 WT
USP10-ΔDUB
USP10-CA
10μm
b
Axin1 puncta numbers per cell
ns
p=0.0416
p<0.0001
p<0.0001
p<0.0001
shCtrl
shUSP10
EV
USP10 WT
USP10 ΔDUB
USP10 CA
c
Axin1 puncta diameter(μm)
p=0.0215
p=0.0012
p<0.0001
p=0.0019
p<0.0001
d
Axin1 Immobile fraction
ns
p<0.0001
p<0.0001
p<0.0057
p=0.0068
e
Axin1-mCherry
DAPI
Merge
Parental
sgUSP10
EV
USP10 WT
USP10 CA
USP10 -ΔDUB
USP10 -ΔDUB -ΔPBR
15μm
SW480
f
Axin1 puncta number
p=0.0012
p=0.0007
p=0.0002
p=0.0003
SW480
Parental
EV
WT
CA
ΔDUB
ΔDUB-ΔPBR
sgUSP10
g
Axin1-mCherry
USP10-GFP
Overlay
Blank
USP10 WT
USP10 CA
USP10-ΔDUB
USP10-ΔDUB-ΔPBR
In vitro droplet
h
In vitro droplet
Axin1 puncta size (μm)
ns
p<0.0001
p<0.0001
p<0.0001
Blank
WT
CA
ΔDUB
ΔDUB-ΔPBR
USP10
i
Immobile fraction
p<0.0001
ns
ns
ns
Axin1 WT +EV
Axin1 DA +EV
Axin1 DA +USP10 WT
Axin1 WT+ USP10 ΔPBR
j
USP10 presence:
Axin1 deubiquitination✓
LLPS escalation✓
Strong inhibition
of Wnt/β-catenin signaling
Enhanced
Interaction between
β-catenin and Axin1
APC
β-catenin
Axin1
RGS
DIX
S1
S2
S4
DUB
USP10
K48-linked Ub
removal from
Axin1
USP10 losing DUB activity:
Axin1 deubiquitination✗
LLPS escalation✓
Moderation inhibition
of Wnt/β-catenin signaling
Enhanced
Interaction between
β-catenin and Axin1
DUB dead
USP10 absence:
Axin1 deubiquitination✗
LLPS escalation✗
No inhibition
of Wnt/β-catenin signaling

Figure 5

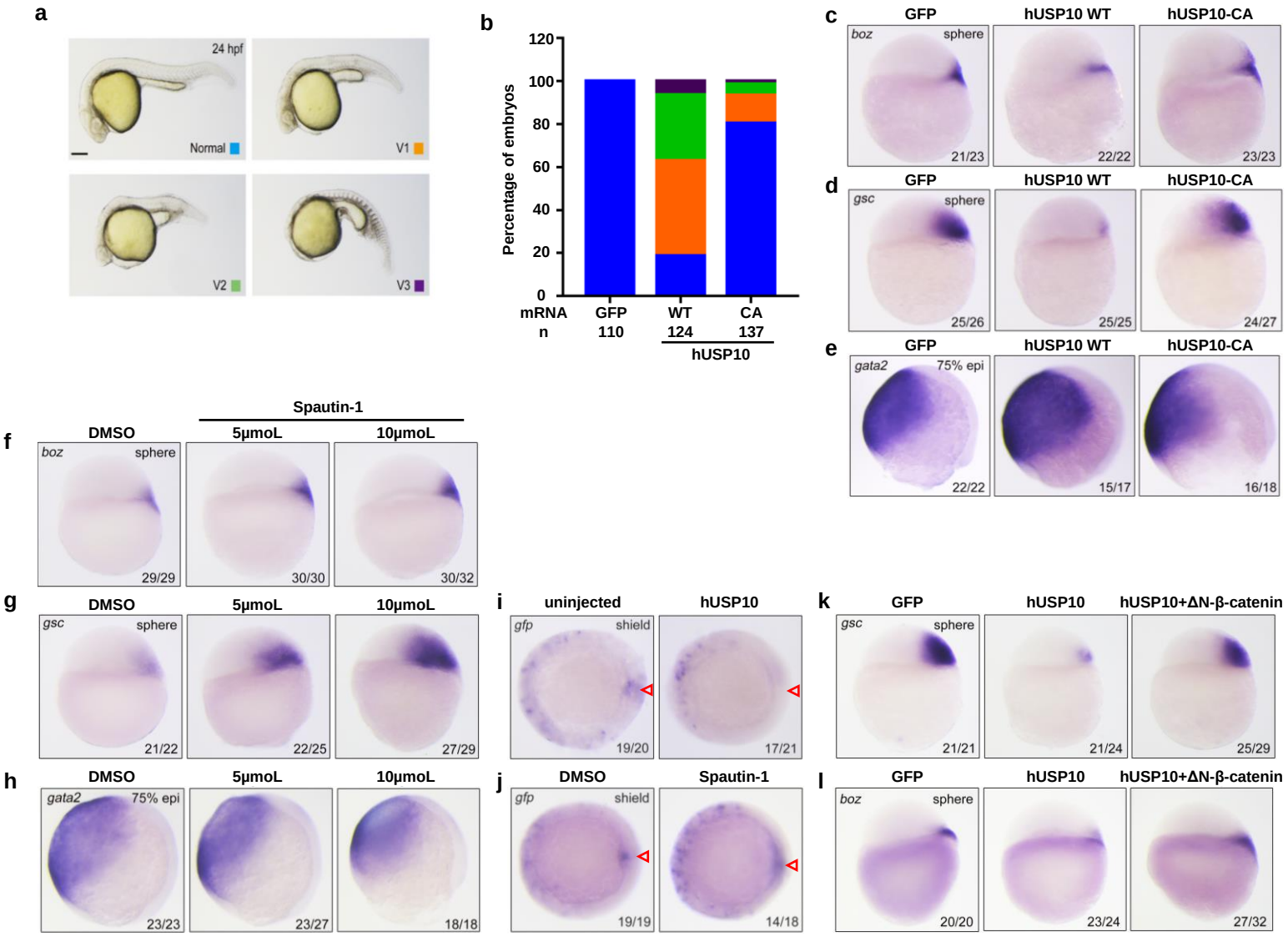
a
24 hpf
Normal
V1
V2
V3
b
Percentage of embryos
120
100
80
60
40
20
0
mRNA
n
GFP
110
WT
124
CA
137
hUSP10
c
GFP
hUSP10 WT
hUSP10-CA
boz
sphere
21/23
22/22
23/23
d
GFP
hUSP10 WT
hUSP10-CA
gsc
sphere
25/26
25/25
24/27
e
GFP
hUSP10 WT
hUSP10-CA
gata2
75% epi
22/22
15/17
16/18
f
Spautin-1
DMSO
5μmoL
10μmoL
boz
sphere
29/29
30/30
30/32
g
DMSO
5μmoL
10μmoL
gsc
sphere
21/22
22/25
27/29
h
DMSO
5μmoL
10μmoL
gata2
75% epi
23/23
23/27
18/18
i
uninjected
hUSP10
gfp
shield
19/20
17/21
j
DMSO
Spautin-1
gfp
shield
19/19
14/18
k
GFP
hUSP10
hUSP10+ΔN-β-catenin
gsc
sphere
21/21
21/24
25/29
l
GFP
hUSP10
hUSP10+ΔN-β-catenin
boz
sphere
20/20
23/24
27/32

Figure 6

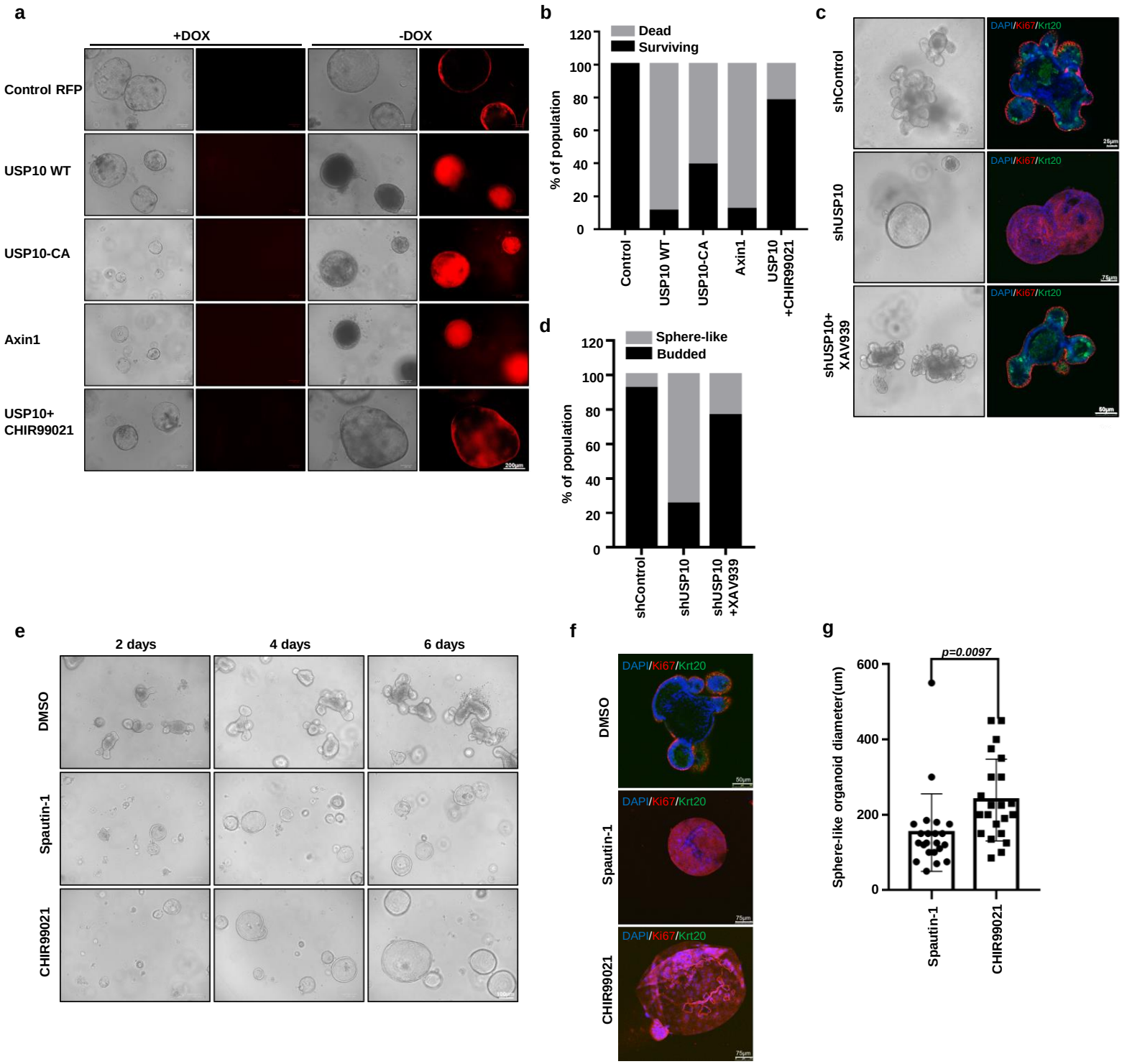
a
+DOX
-DOX
Control RFP
USP10 WT
USP10-CA
Axin1
USP10+
CHIR99021
200μm
b
Dead
Surviving
% of population
120
100
80
60
40
20
0
Control
USP10 WT
USP10-CA
Axin1
USP10
+CHIR99021
c
shControl
shUSP10
shUSP10+
XAV939
DAPI/Ki67/Krt20
25μm
75μm
50μm
d
Sphere-like
Budded
% of population
120
100
80
60
40
20
0
shControl
shUSP10
shUSP10
+XAV939
e
2 days
4 days
6 days
DMSO
Spautin-1
CHIR99021
100μm
f
DMSO
Spautin-1
CHIR99021
DAPI/Ki67/Krt20
50μm
75μm
g
p=0.0097
Sphere-like organoid diameter(um)
600
400
200
0
Spautin-1
CHIR99021

Figure 7

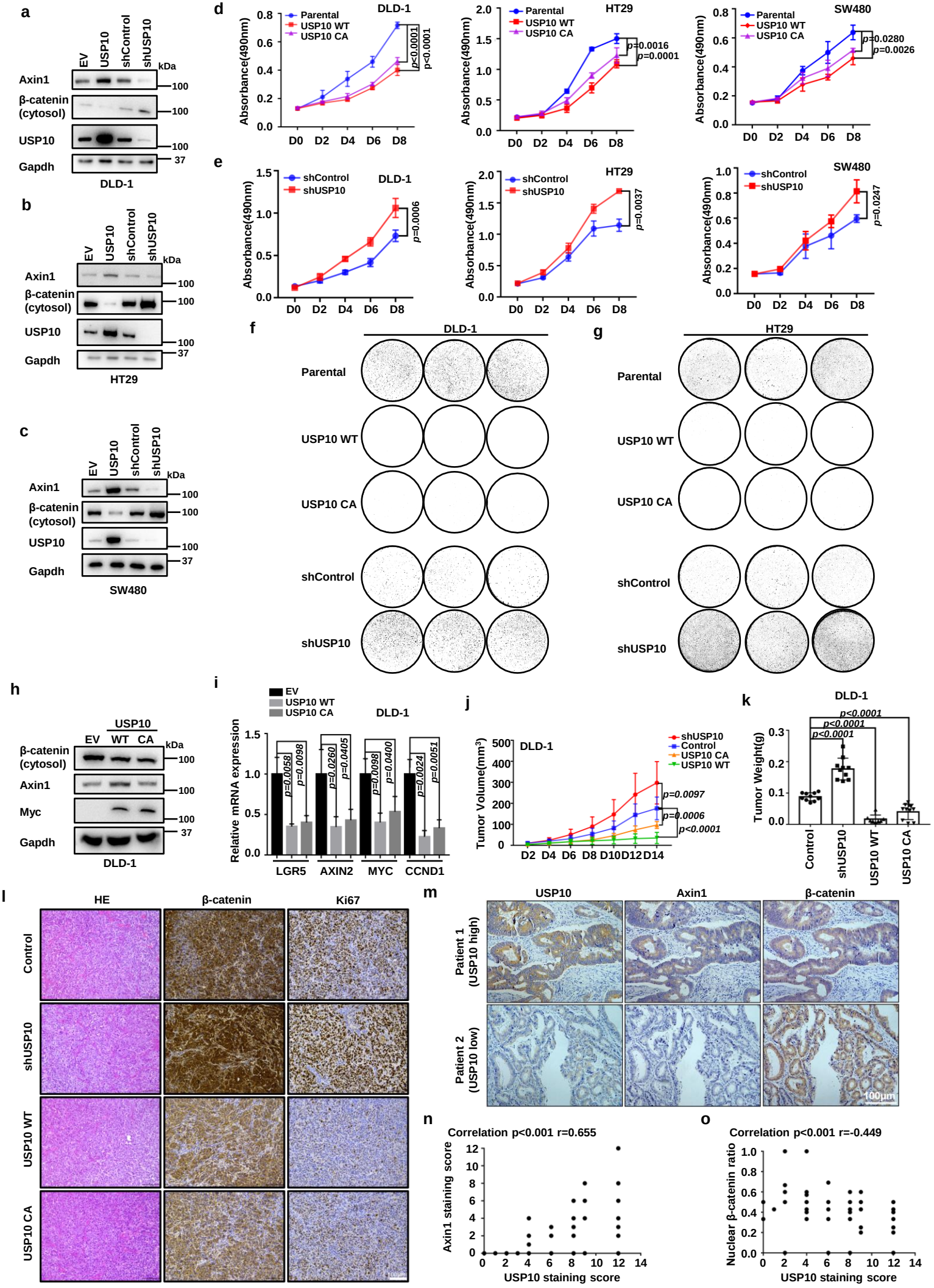
a
EV
USP10
shControl
shUSP10
kDa
Axin1
β-catenin (cytosol)
USP10
Gapdh
100
37
DLD-1
b
HT29
c
SW480
d
DLD-1
HT29
SW480
Parental
USP10 WT
USP10 CA
Absorbance(490nm)
D0 D2 D4 D6 D8
p<0.0001
p=0.0016
p=0.0280
p=0.0026
e
shControl
shUSP10
p=0.0006
p=0.0037
p=0.0247
f
g
h
USP10
EV WT CA
Myc
i
EV
USP10 WT
USP10 CA
Relative mRNA expression
LGR5
AXIN2
MYC
CCND1
p=0.0058
p=0.0098
p=0.0260
p=0.0405
p=0.0098
p=0.0400
p=0.0024
p=0.0051
j
Tumor Volume(mm³)
shUSP10
Control
USP10 CA
USP10 WT
D2 D4 D6 D8 D10 D12 D14
p=0.0097
p=0.0006
p<0.0001
k
Tumor Weight(g)
Control
shUSP10
USP10 WT
USP10 CA
l
HE
β-catenin
Ki67
Control
shUSP10
USP10 WT
USP10 CA
m
USP10
Axin1
β-catenin
Patient 1 (USP10 high)
Patient 2 (USP10 low)
100μm
n
Correlation p<0.001 r=0.655
Axin1 staining score
USP10 staining score
o
Correlation p<0.001 r=-0.449
Nuclear β-catenin ratio
USP10 staining score

Supplementary Figure 1

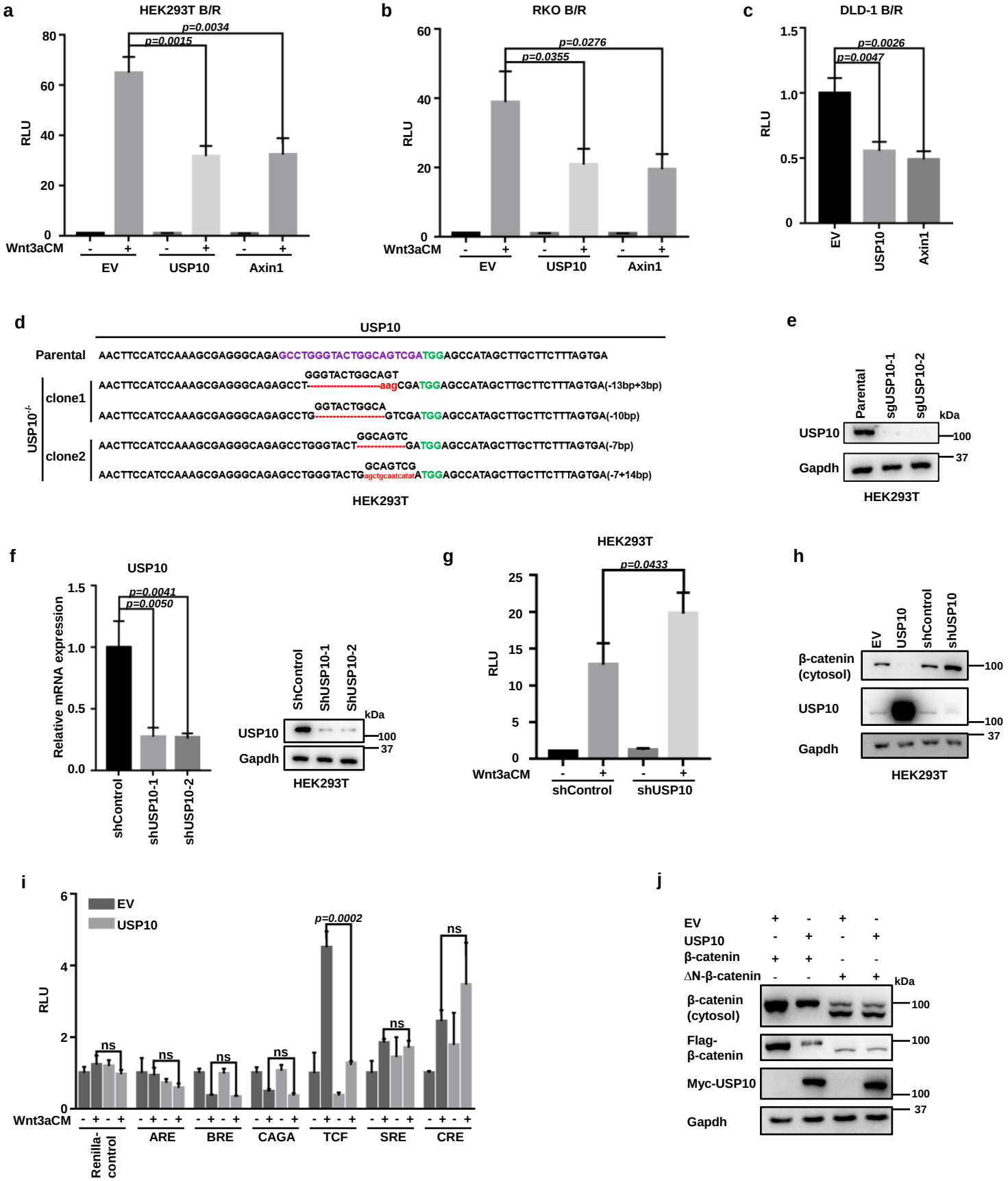

Supplementary Figure 2

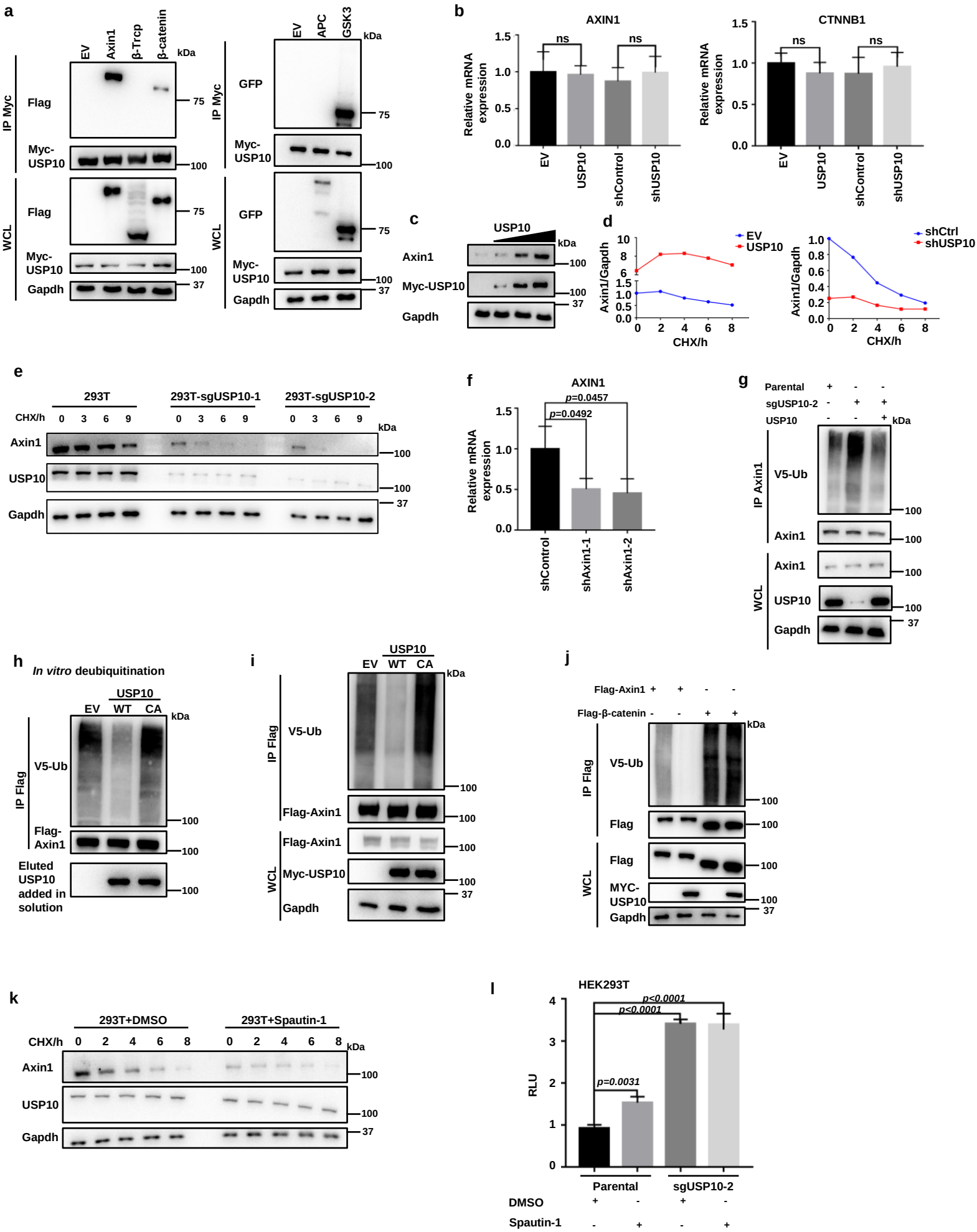

Supplementary Figure 3

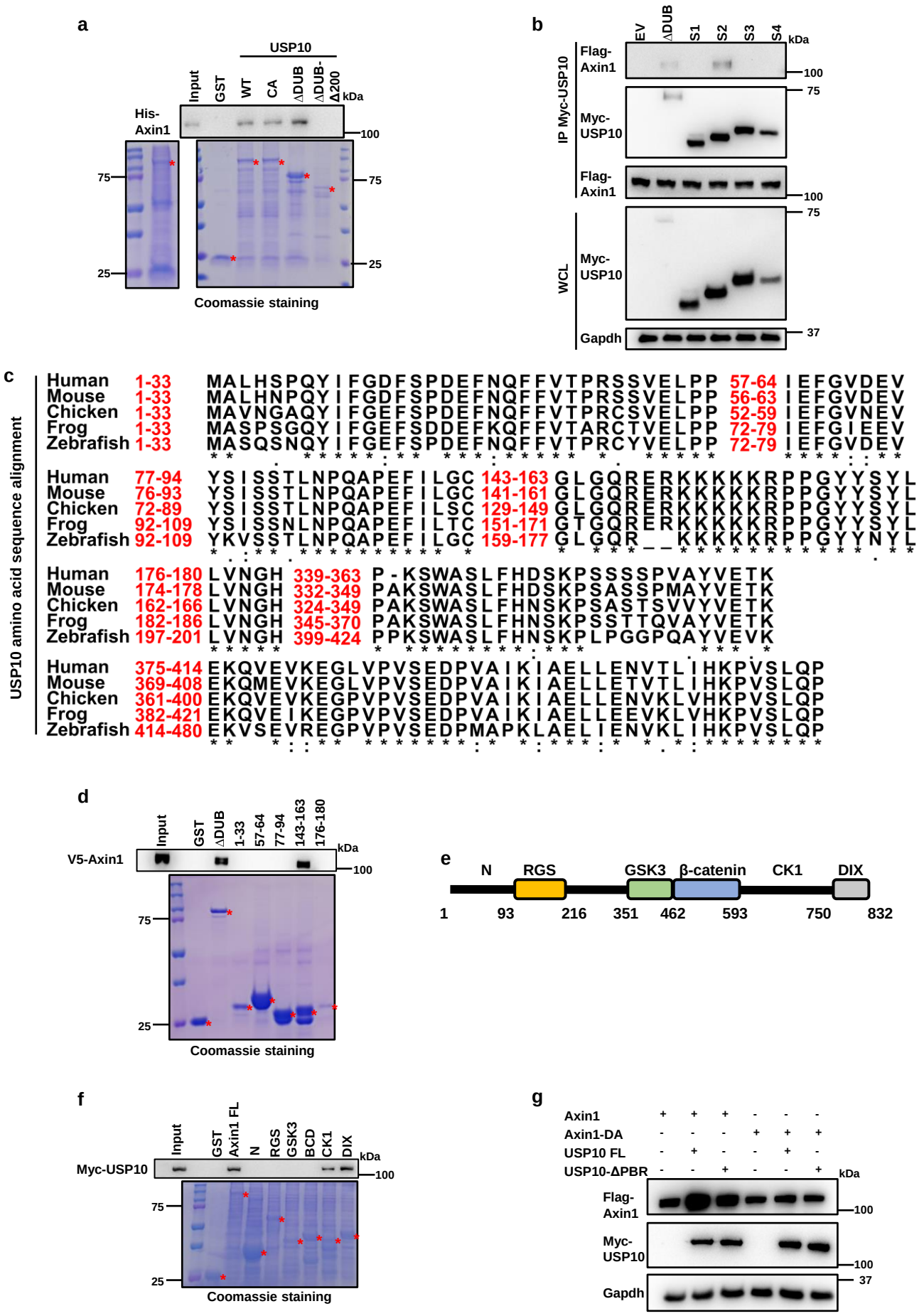

Supplementary Figure 4

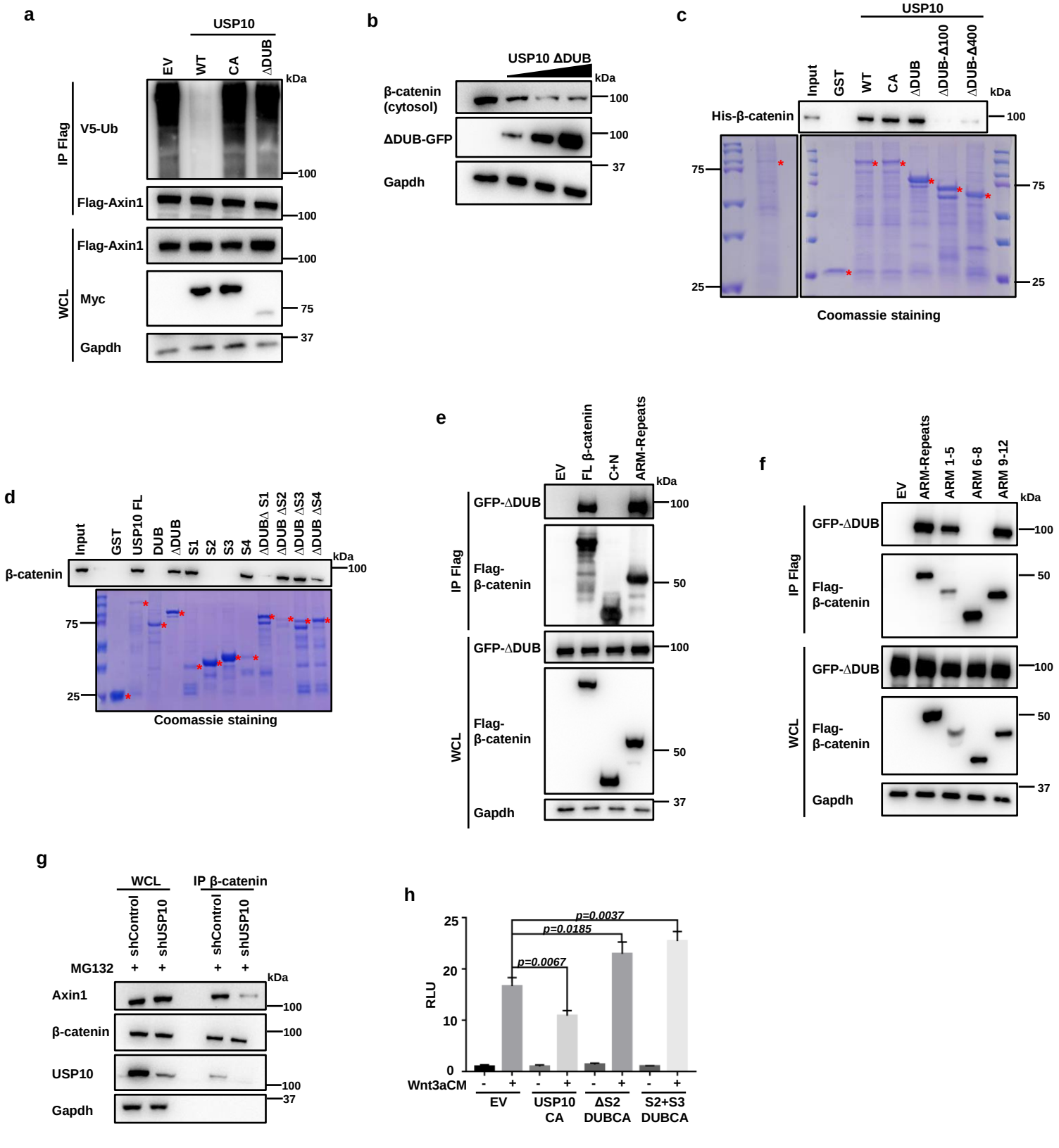

Supplementary Figure 5

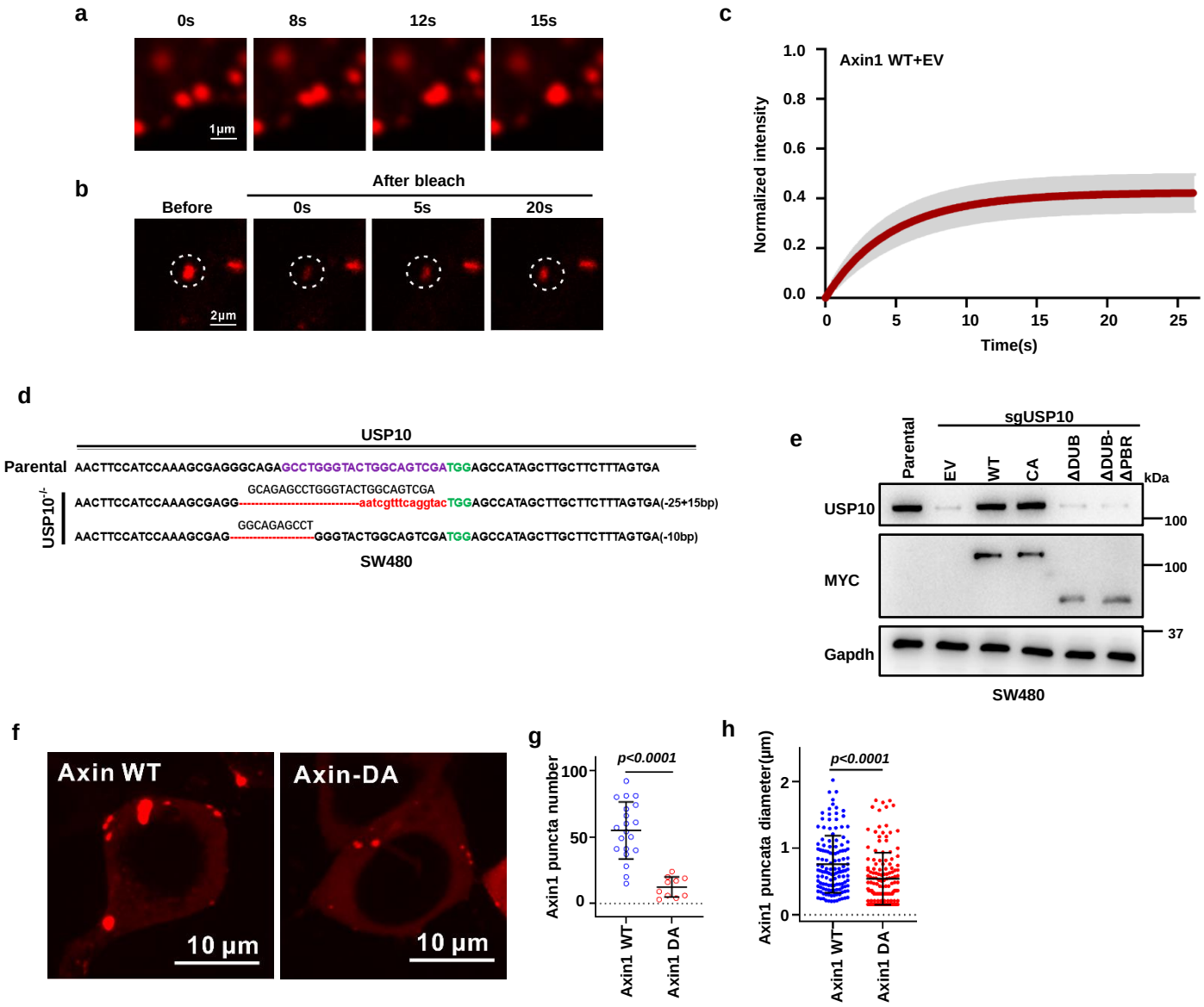

Supplementary Figure 6

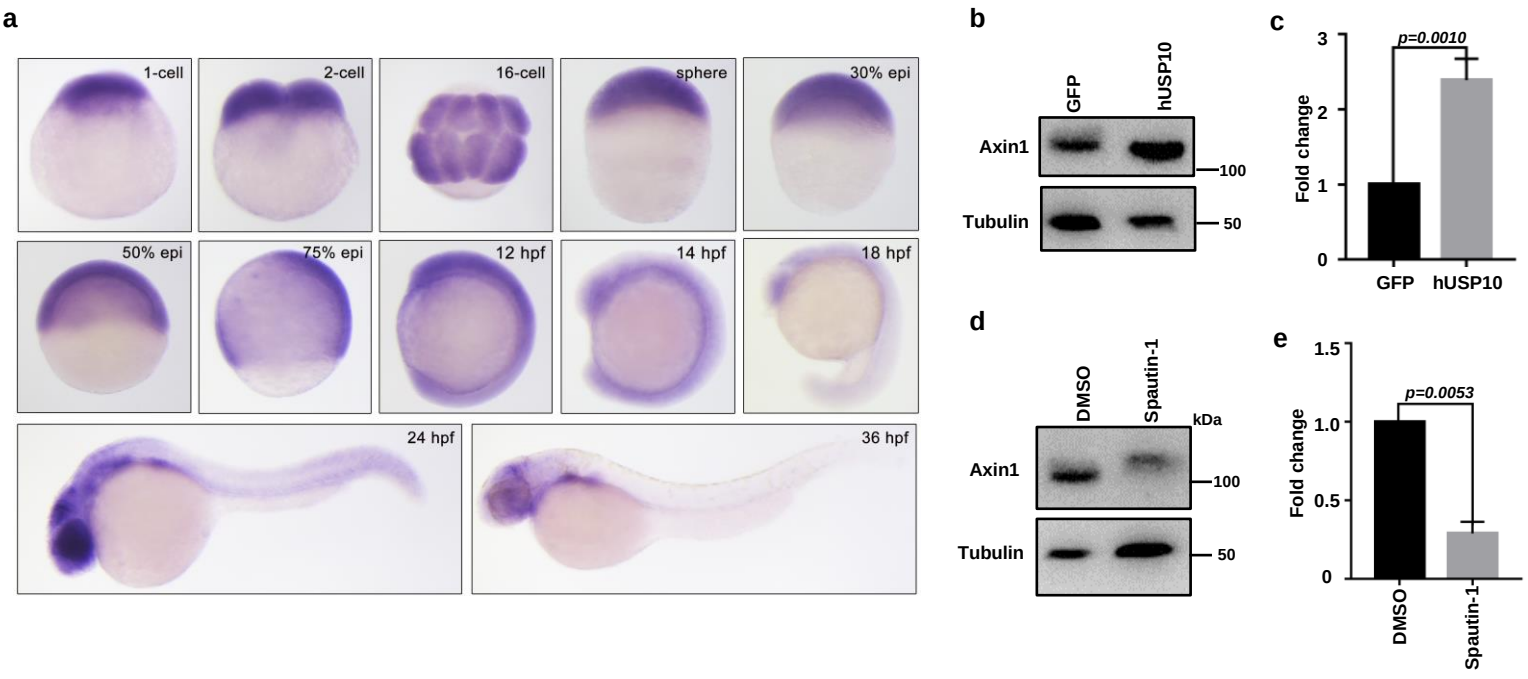

Supplemental Figure 7

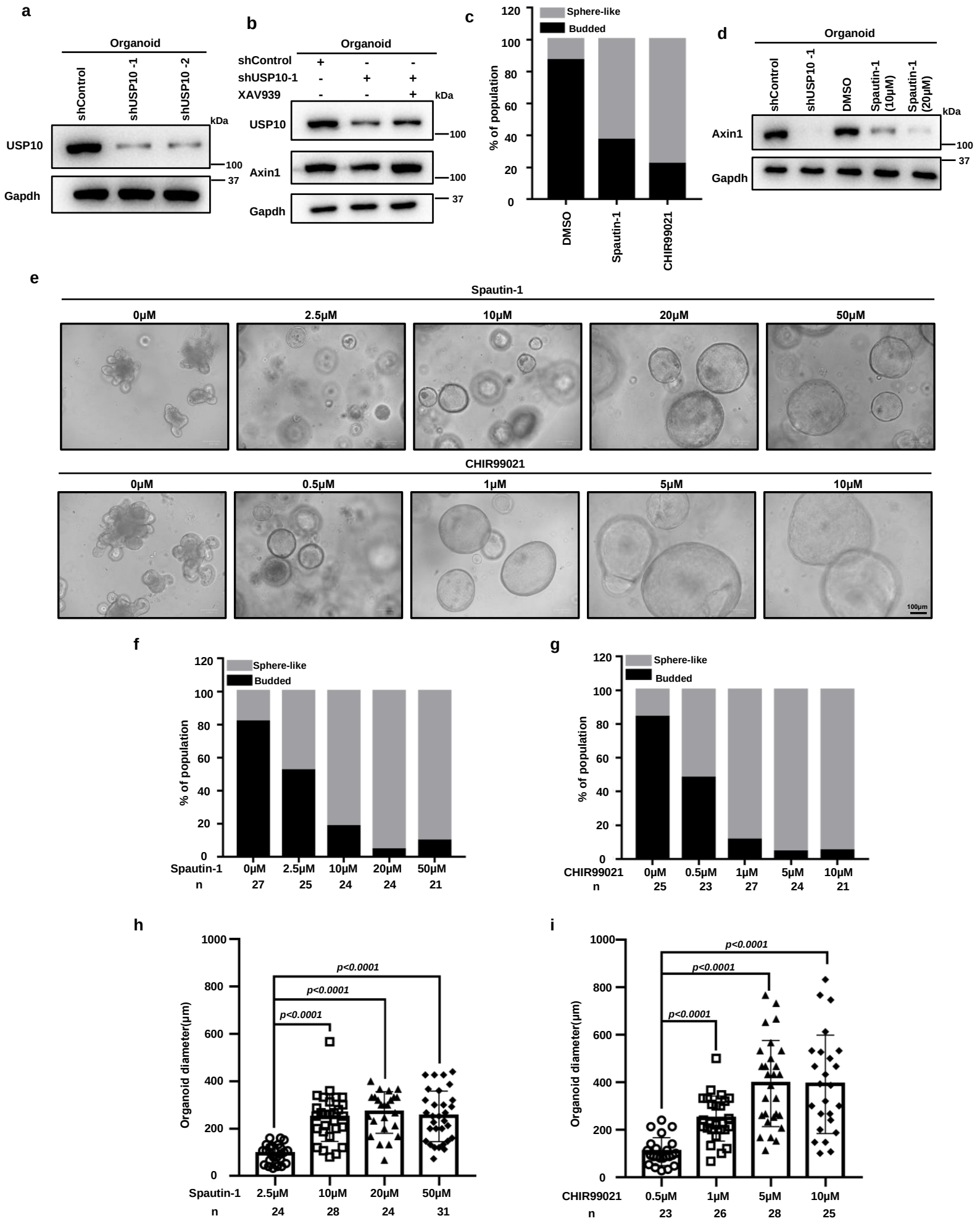
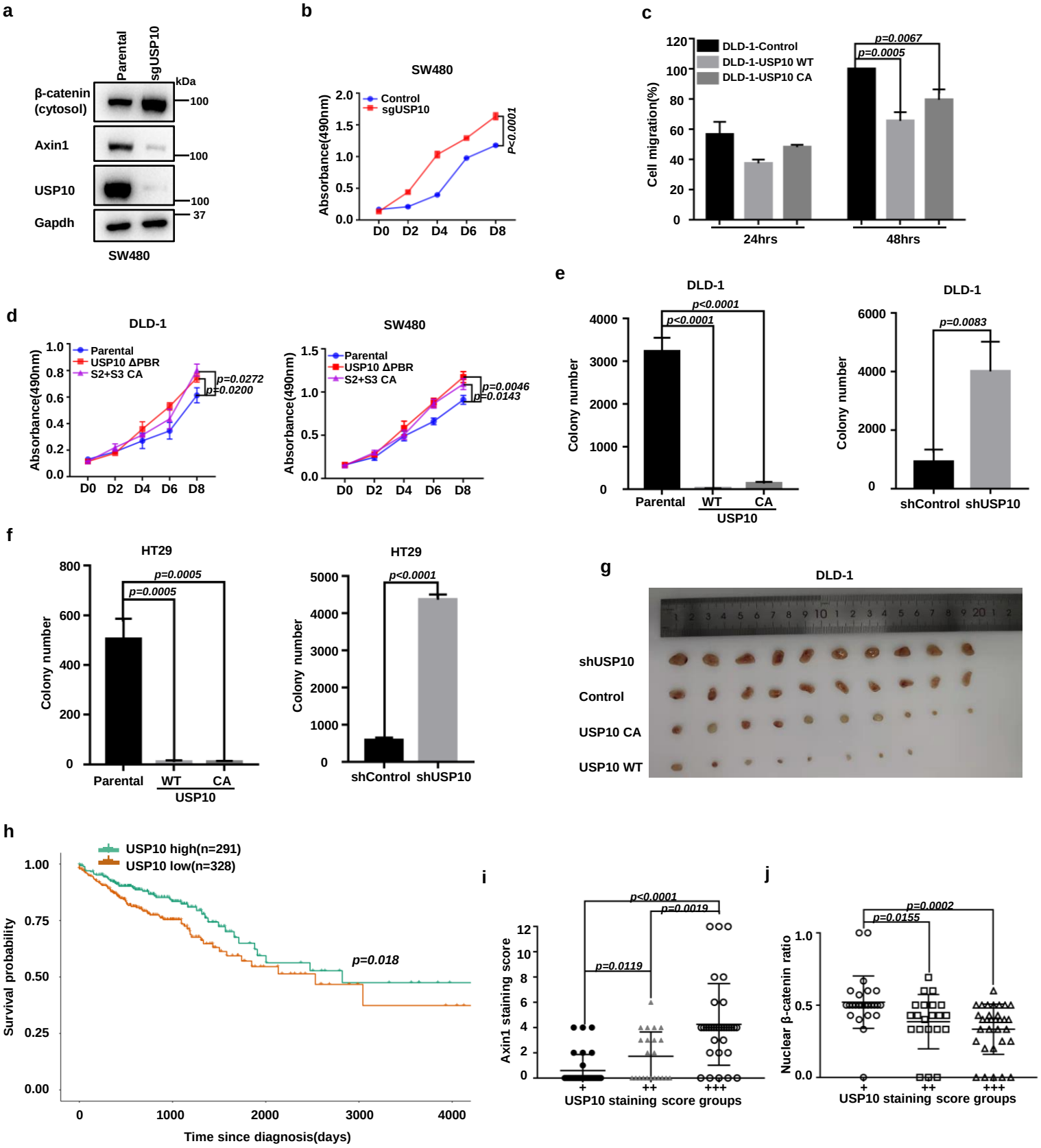
Supplementary Figure 8